SUPPLEMENTARY MATERIALS

Quantifying Causal Contributions in Earth Systems by Normalized Information Flow

Chin-Hsien Cheng[1,2], Simon A. T. Redfern[1]

[1]Asian School of the Environment, Nanyang Technological University, 50 Nanyang Avenue, Singapore 639798
[2]Joint International Research Laboratory of Climate and Environment Change, Nanjing University of Information Science and Technology (NUIST), Nanjing 210044, China

Correspondence to: Simon A. T. Redfern (simon.redfern@ntu.edu.sg)

Data Processing

The “multipliers” given in equation 16 between designed variables X and Y have been estimated over a moving time range. The estimated multiplier is then multiplied by the rate of change of cause-variable at the middle of the time-window so that the causal contribution can be estimated using equation 16. For the 1D tests, each time range spans 100 time-units, while for the 3D tests, each window consists of only 49 time-units. For example, this might be a common timeframe for studying interannual variability of monthly data (i.e. 49 months in total, representing a centered month ± 24 months).

In Fig. 3a-d, i-p, a 21-time-unit lag between coupled feedback is introduced for time t >200. In other words, from $t = 201$ onwards, $\partial X(Y)/\partial t$ at time t is set to be a function of Y from 21 time-units previously, and similarly $\partial Y(X)/\partial t$ at time t becomes a function of X from 21 time-units prior. This time-lag corresponds to 21% of the 100 unit moving timeframe used in each analysis, in contrast to tests in Fig. 2 where the influence from cause- to effect- variables takes place at the immediately following time step (i.e. with only 1-unit (or 1%) time lag). Similarly, in Fig. 3e-h, a 21-time-unit lag is set for the self-consistency terms, and in Fig. 3q-t, a reverse 31-time-unit gap (effects leading causes) between the interdependent terms is examined. For the reverse causality test, the designed functions remove the self-dependency terms since this has been shown to introduce errors to the estimates given by both IF_a and various nIF_as. The reversed time coupled feedbacks are calculated over 20 iterations with a 31-unit reverse time-gap based on preliminary calculated results from the standard 1-unit-time-lag as iteration 0. However, such reversed time-gaps are even harder to capture than the ordinary time-lags. Note that the functions tested in Fig. 3 are almost the same with only minor changes to evaluate the corresponding effect.

In Fig. 5, the results are estimated based on equations 18-24. In addition to splitting the higher order of causal dependency into two first-order equations (18-20), the key is to have a preliminary removal of independent noise and $\partial X_{long}(Y)/\partial t$ (through equations 22-24) for better estimates of the $\partial X_{hys}(Y)/\partial t$ (Fig. S16, S18, S20 vs S15, S17, and S19). Within the running window of 100 time-units, the dX_{ref}/dt is assumed to be the running mean of dX/dt at ~25th time-unit (i.e. 25% from the beginning of the running window, equation 24). The key here is to remove the growing $\partial X_{long}(Y)/\partial t$ so that the dX_{ref}/dt must be dynamically moved with the running window. There is no perfect choice for the position of dX_{ref}/dt in the running window. A position nearer to the beginning of the running window may leave more influence of growing $\partial X_{long}(Y)/\partial t$ unfiltered in the dX_{adj}/dt and hence the X_{adj}. However, a position nearer to the end or just the mid-point of the running time window may cause over-removal of $\partial X(noise)/\partial t$ and $\partial X_{long}(Y)/\partial t$, resulting in a potential wrong correlation sign between the X_{adj} and Y. The chosen 25% allows most (75%) datapoints of dX_{adj}/dt to fall behind the dX_{ref}/dt to reflect the hysteresis causal effect on $\partial X_{hys}(Y)/\partial t$, limiting the chance of wrong correlation sign, while possibly filtering most influence from $\partial X(noise)/\partial t$ and $\partial X_{long}(Y)/\partial t$. Nevertheless, this 25-75% cut is not optimized, since the optimal cut is likely depending on the causal functions. For example, the same 25-75% cut for dY_{adj}/dt and Y_{adj} to run the causal analysis with the X, tends to significantly introduce wrong correlation sign and affect the estimates of $\partial Y(X)/\partial t$ (Fig. S20 vs S19). This leaves room of improvement for the suggested method.

Table S1. Designed functions assessed with results presented in the Figures

Fig. #	Interdependent function	Noise function (inc. self-dependency)
One-Dimensional: nt = 2 to 1000; (or split into 2-200, 201-1000) initial conditions (i.e. nt = 1) are zeros; $\vert_{nt}$ or $\vert_{nt-1}$ refers to nt^{th} or $(nt\text{-}1)^{th}$ term on time-axis		
2a-d, 5a-h (S1,S15,S16): single directional causality, constant noise	$\left.\frac{\partial X_1(Y_1)}{\partial t}\right\|_{nt} = \left\{\frac{\cos\left[\frac{\left(2nt+\sum_2^{nt}\frac{1}{nt}\right)}{120\pi}\right]}{\mathbf{1.1}} + \frac{\sin\left[\frac{\left(2nt-\sum_2^{nt}\frac{1}{nt}\right)}{120\pi}\right]}{\mathbf{1.5}} + \frac{1}{\mathbf{3}}\right\}\left.\frac{dY_1}{dt}\right\|_{nt-1}$ $\left.\frac{\partial Y_1(X_1)}{\partial t}\right\|_{nt} = 0$	$\left.\frac{\partial X_1(noise)}{\partial t}\right\|_{nt} = \mathbf{0.1}$ $\left.\frac{\partial Y_1(noise)}{\partial t}\right\|_{nt} = \mathbf{-0.05}$
2e-h (S2): single directional causality, oscillating noise with high independent noise-to-signal ratio	$\left.\frac{\partial X_1(Y_1)}{\partial t}\right\|_{nt} = \left\{\frac{\cos\left[\frac{\left(2nt+\sum_2^{nt}\frac{1}{nt}\right)}{120\pi}\right]}{8} + \frac{\sin\left[\frac{\left(2nt-\sum_2^{nt}\frac{1}{nt}\right)}{140\pi}\right]}{\mathbf{10}} + \frac{1}{20}\right\}\left.\frac{dY_1}{dt}\right\|_{nt-1}$ $\left.\frac{\partial Y_1(X_1)}{\partial t}\right\|_{nt} = 0$	$\left.\frac{\partial X_1(noise)}{\partial t}\right\|_{nt} = \mathbf{0.65} - \frac{\cos\left(\frac{4nt}{\mathbf{200}\pi}\right)}{\mathbf{2}} + \sin\left(\frac{6nt}{\mathbf{200}\pi}\right)$ $\left.\frac{\partial Y_1(noise)}{\partial t}\right\|_{nt} = \mathbf{-0.05} - \frac{\sin\left(\frac{2nt}{\mathbf{300}\pi}\right)}{\mathbf{2}} + \cos\left(\frac{3nt}{\mathbf{250}\pi}\right)$
2i-l (S3): single directional causality, oscillating self-dependent noise	$\left.\frac{\partial X_1(Y_1)}{\partial t}\right\|_{nt} = \left\{\frac{\cos\left[\frac{\left(1.2nt+\sum_2^{nt}\frac{1}{nt}\right)}{120\pi}\right]}{1.9} + \frac{\sin\left[\frac{\left(1.5nt-\sum_2^{nt}\frac{1}{nt}\right)}{140\pi}\right]}{\mathbf{2.3}} + \frac{1}{4.9}\right\}\left.\frac{dY_1}{dt}\right\|_{nt-1}$ $\left.\frac{\partial Y_1(X_1)}{\partial t}\right\|_{nt} = 0$	$\left.\frac{\partial X_1(noise)}{\partial t}\right\|_{nt} = \left[\mathbf{-0.44} - \frac{\cos\left(\frac{4nt}{\mathbf{200}\pi}\right)}{\mathbf{7}} + \frac{\sin\left(\frac{6nt}{\mathbf{200}\pi}\right)}{5}\right] X_1\|_{nt-1}$ $\left.\frac{\partial Y_1(noise)}{\partial t}\right\|_{nt} = \mathbf{0.6} + \left[\mathbf{-0.4} - \frac{\sin\left(\frac{5nt}{\mathbf{300}\pi}\right)}{\mathbf{6}} + \frac{\cos\left(\frac{7nt}{\mathbf{250}\pi}\right)}{6}\right] Y_1\|_{nt-1}$
2m-p (S4): coupled feedback loop with very weak noise	$\left.\frac{\partial X_1(Y_1)}{\partial t}\right\|_{nt} = \left\{\frac{\cos\left[\frac{\left(2nt+\sum_2^{nt}\frac{1}{nt}\right)}{120\pi}\right]}{1.4} + \frac{\sin\left[\frac{\left(2.5nt-\sum_2^{nt}\frac{1}{nt}\right)}{140\pi}\right]}{\mathbf{1.7}} + \frac{1}{2}\right\}\left.\frac{dY_1}{dt}\right\|_{nt-1}$ $\left.\frac{\partial Y_1(X_1)}{\partial t}\right\|_{nt} = \frac{1}{3}\left.\frac{dX_1}{dt}\right\|_{nt-1}$	$\left.\frac{\partial X_1(noise)}{\partial t}\right\|_{nt} = \mathbf{0.052} - \frac{\cos\left(\frac{4nt}{\mathbf{200}\pi}\right)}{\mathbf{60}} + \frac{\sin\left(\frac{6nt}{\mathbf{200}\pi}\right)}{\mathbf{65}} - \frac{X_1\|_{nt-1}}{100}$ $\left.\frac{\partial Y_1(noise)}{\partial t}\right\|_{nt} = \mathbf{-0.044} + \frac{\cos\left(\frac{3nt}{\mathbf{250}\pi}\right)}{\mathbf{35}} - \frac{\sin\left(\frac{2nt}{\mathbf{300}\pi}\right)}{\mathbf{30}} - \frac{Y_1\|_{nt-1}}{95}$
2q-t (S5): – coupled feedback loop with strong oscillating independent noise that often changes its	$\left.\frac{\partial X_1(Y_1)}{\partial t}\right\|_{nt} = \left\{\frac{\cos\left[\frac{\left(2nt+\sum_2^{nt}\frac{1}{nt}\right)}{120\pi}\right]}{1.9} + \frac{\sin\left[\frac{\left(2.5nt-\sum_2^{nt}\frac{1}{nt}\right)}{140\pi}\right]}{\mathbf{2.3}} + \frac{1}{490}\right\}\left.\frac{dY_1}{dt}\right\|_{nt-1}$	$\left.\frac{\partial X_1(noise)}{\partial t}\right\|_{nt} = \mathbf{0.26} + \left\|\frac{\cos\left(\frac{1.5nt}{\mathbf{200}\pi}\right)}{\mathbf{1.9}}\right\| - \left\|\frac{\sin\left(\frac{nt}{\mathbf{200}\pi}\right)}{\mathbf{2}}\right\|$

<table>
<tr><td>direction suddenly</td><td>$$\left.\frac{\partial Y_1(X_1)}{\partial t}\right|_{nt} = \left\{\frac{cos\left[\frac{\left(nt+\sum_2^{nt}\frac{1}{nt}\right)}{310\pi}\right]}{2.4} + \frac{sin\left[\frac{\left(1.8nt-\sum_2^{nt}\frac{1}{nt}\right)}{240\pi}\right]}{\mathbf{2.9}} + \frac{1}{600}\right\}\left.\frac{dX_1}{dt}\right|_{nt-1}$$</td><td>$$\left.\frac{\partial Y_1(noise)}{\partial t}\right|_{nt} = \mathbf{0.2} + \left|\frac{sin\left(\frac{1.2nt}{\mathbf{300}\pi}\right)}{\mathbf{2.2}}\right| - \left|\frac{cos\left(\frac{1.5nt}{\mathbf{250}\pi}\right)}{\mathbf{2.4}}\right|$$</td></tr>
<tr><td>3a-d (S6): 21-unit time-gap between interdependency terms</td><td>$$\left.\frac{\partial X_1(Y_1)}{\partial t}\right|_{nt} = \left\{\frac{cos\left[\frac{\left(2nt+\sum_2^{nt}\frac{1}{nt}\right)}{120\pi}\right]}{1.9} + \frac{sin\left[\frac{\left(2.5nt-\sum_2^{nt}\frac{1}{nt}\right)}{140\pi}\right]}{\mathbf{2.3}} + \frac{1}{4.9}\right\}\left.\frac{dY_1}{dt}\right|_{nt-1}$$
$$\left.\frac{\partial Y_1(X_1)}{\partial t}\right|_{nt} = \left\{\frac{cos\left[\frac{\left(nt+\sum_2^{nt}\frac{1}{nt}\right)}{310\pi}\right]}{2.4} + \frac{sin\left[\frac{\left(1.8nt-\sum_2^{nt}\frac{1}{nt}\right)}{240\pi}\right]}{\mathbf{2.9}} + \frac{1}{6}\right\}\left.\frac{dX_1}{dt}\right|_{nt-1}$$
For nt >200, change $\left.\frac{dY1}{dt}\right|_{nt-1}$ to $\left.\frac{dY1}{dt}\right|_{nt-21}$, $\left.\frac{dX1}{dt}\right|_{nt-1}$ to $\left.\frac{dX1}{dt}\right|_{nt-21}$</td><td>$$\left.\frac{\partial X_1(noise)}{\partial t}\right|_{nt} = \mathbf{0.26} - \frac{cos\left(\frac{3nt}{\mathbf{200}\pi}\right)}{\mathbf{10}} + \frac{sin\left(\frac{6nt}{\mathbf{200}\pi}\right)}{\mathbf{15}} - \frac{X_1|_{nt-1}}{40}$$
$$\left.\frac{\partial Y_1(noise)}{\partial t}\right|_{nt} = -\mathbf{0.2} + \frac{cos\left(\frac{3nt}{\mathbf{250}\pi}\right)}{\mathbf{15}} - \frac{sin\left(\frac{2nt}{\mathbf{300}\pi}\right)}{\mathbf{10}} - \frac{Y_1|_{nt-1}}{30}$$</td></tr>
<tr><td>S7: control test</td><td>Same as in Fig. S6, except keeping the $\left.\frac{dY1}{dt}\right|_{nt-1}$ and $\left.\frac{dX1}{dt}\right|_{nt-1}$ throughout</td><td>Same as in Fig. S6</td></tr>
<tr><td>3e-h (S8)</td><td>Same as in Fig. S6</td><td>Same as in Fig. S6, except changing the $\left.\frac{dY1}{dt}\right|_{nt-1}$ to $\left.\frac{dY1}{dt}\right|_{nt-21}$, $\left.\frac{dX1}{dt}\right|_{nt-1}$ to $\left.\frac{dX1}{dt}\right|_{nt-21}$ when nt >200</td></tr>
<tr><td>3i-l (S9)</td><td>Same as in Fig. S6 and S8</td><td>Same as in Fig. S8</td></tr>
<tr><td>3m-p (S10)</td><td>Same as in Fig. S6 and S8</td><td>Same as in Fig. S8, except changing the 3nt of the cosine term for $\left.\frac{\partial X_1(noise)}{\partial t}\right|_{nt}$ into 4nt</td></tr>
<tr><td>3q-t (S11)</td><td>Same as in Fig. S6, except changing $\left.\frac{dY1}{dt}\right|_{nt-21}$ to $\left.\frac{dY1}{dt}\right|_{nt+31}$, $\left.\frac{dX1}{dt}\right|_{nt-21}$ to $\left.\frac{dX1}{dt}\right|_{nt+31}$ when nt >200

20 rounds of iteration to obtain a converged dataset for the time-reversed causality</td><td>$$\left.\frac{\partial X_1(noise)}{\partial t}\right|_{nt} = \mathbf{0.13} - \frac{cos\left(\frac{1.5nt}{\mathbf{200}\pi}\right)}{\mathbf{10}} + \frac{sin\left(\frac{2nt}{\mathbf{200}\pi}\right)}{\mathbf{15}}$$
$$\left.\frac{\partial Y_1(noise)}{\partial t}\right|_{nt} = -\mathbf{0.1} + \frac{cos\left(\frac{3nt}{\mathbf{250}\pi}\right)}{\mathbf{15}} - \frac{sin\left(\frac{2nt}{\mathbf{300}\pi}\right)}{\mathbf{10}}$$
Similar to Fig. S6, with reduced magnitude and frequency</td></tr>
<tr><td colspan="3">Three-Dimensional (nlon, nlat, t) with nlon = 1 to 360, nlat = 1 to 180 in loop calculations
initial conditions (t = 1) are zeros;
for N-S teleconnection, the cause-variable are from 181-nlat</td></tr>
<tr><td>4 & S13 N-S tele-connection</td><td>$$\left.\frac{\partial X(Y)}{\partial t}\right|_{t,nlon,nlat} = \left\{\frac{cos\left[\frac{nlon+2t}{\mathbf{270}\pi}\right]}{\mathbf{9}} + \frac{sin\left[\frac{(\mathbf{181}-\boldsymbol{nlat})+3t}{\mathbf{280}\pi}\right]}{\mathbf{10}} + \frac{1}{\mathbf{3}}\right\}\left.\frac{dY}{dt}\right|_{t-1,nlon,\mathbf{181}-\boldsymbol{nlat}}$$</td><td>$$\left.\frac{\partial X(noise)}{\partial t}\right|_{t,nlon,nlat} = \mathbf{0.03} + \left|\frac{cos\left(\frac{nlon+\mathbf{5}t}{\mathbf{320}\pi}\right)}{\mathbf{1.2}}\right| + \left|\frac{sin\left(\frac{nlat+\mathbf{8}t}{\mathbf{330}\pi}\right)}{\mathbf{2}}\right|$$</td></tr>
</table>

	$\left.\frac{\partial Y(X)}{\partial t}\right\|_{t,nlon,nlat} = \left\{\frac{cos\left[\frac{nlon+3t}{290\pi}\right]}{9} + \frac{sin\left[\frac{(181-nlat)+2t}{260\pi}\right]}{4} + \frac{1}{1.4}\right\}\left.\frac{dX}{dt}\right\|_{t-1,nlon,181-nlat}$	$\left.\frac{\partial Y(noise)}{\partial t}\right\|_{t,nlon,nlat} = 0.02 + \left\|\frac{cos\left(\frac{nlon+4t}{350\pi}\right)}{2}\right\| + \left\|\frac{sin\left(\frac{nlat+12t}{340\pi}\right)}{3}\right\|$
S12 & S14 no tele-connection	$\left.\frac{\partial X(Y)}{\partial t}\right\|_{t,nlon,nlat} = \left\{\frac{cos\left[\frac{nlon+2t}{240\pi}\right]}{8} + \frac{sin\left[\frac{nlat+2t}{250\pi}\right]}{9} + \frac{1}{4}\right\}\left.\frac{dY}{dt}\right\|_{t-1,nlon,nlat}$ $\left.\frac{\partial Y(X)}{\partial t}\right\|_{t,nlon,nlat} = \left\{\frac{cos\left[\frac{nlon+4t}{230\pi}\right]}{3.5} + \frac{sin\left[\frac{nlat+2t}{260\pi}\right]}{2.5} + \frac{1}{1.5}\right\}\left.\frac{dX}{dt}\right\|_{t-1,nlon,nlat}$	$\left.\frac{\partial X(noise)}{\partial t}\right\|_{t,nlon,nlat} = 0.0005 + \left\|\frac{cos\left(\frac{nlon+4t}{220\pi}\right)}{1.2}\right\| + \left\|\frac{sin\left(\frac{nlat+4t}{210\pi}\right)}{1.1}\right\|$ $\left.\frac{\partial Y(noise)}{\partial t}\right\|_{t,nlon,nlat} = 0.001 + \left\|\frac{cos\left(\frac{nlon+10t}{230\pi}\right)}{1.7}\right\| + \left\|\frac{sin\left(\frac{nlat+2t}{200\pi}\right)}{2.5}\right\|$
5i-p (S17, S18): single directional causality with two orders, constant noise	$\left.\frac{\partial X_1(Y_1)}{\partial t}\right\|_{nt,hys} = \left\{\frac{cos\left[\frac{\left(2nt+\sum_2^{nt}\frac{1}{nt}\right)}{120\pi}\right]}{1.1} + \frac{sin\left[\frac{\left(2nt-\sum_2^{nt}\frac{1}{nt}\right)}{120\pi}\right]}{1.5} + \frac{1}{3}\right\}\left.\frac{dY_1}{dt}\right\|_{nt-1}$ $\left.\frac{\partial X_1(Y_1)}{\partial t}\right\|_{nt,long} = Y_{1_{nt-1}}/200$ $\left.\frac{\partial Y_1(X_1)}{\partial t}\right\|_{nt} = 0$	$\left.\frac{\partial X_1(noise)}{\partial t}\right\|_{nt} = 0.1$ $\left.\frac{\partial Y_1(noise)}{\partial t}\right\|_{nt} = -0.05$
5q-x (S19-S21): coupled feedback loop with one of direction with two order causality, constant noise	$\left.\frac{\partial X_1(Y_1)}{\partial t}\right\|_{nt,hys} = \left\{\frac{cos\left[\frac{\left(2nt+\sum_2^{nt}\frac{1}{nt}\right)}{120\pi}\right]}{1.1} + \frac{sin\left[\frac{\left(2nt-\sum_2^{nt}\frac{1}{nt}\right)}{120\pi}\right]}{1.5} + \frac{1}{3}\right\}\left.\frac{dY_1}{dt}\right\|_{nt-1}$ $\left.\frac{\partial X_1(Y_1)}{\partial t}\right\|_{nt,long} = Y_{1_{nt-1}}/200$ $\left.\frac{\partial Y_1(X_1)}{\partial t}\right\|_{nt} = \left\{\frac{cos\left[\frac{(nt)}{310\pi}\right]}{1.8} - \frac{sin\left[\frac{(nt)}{120\pi}\right]}{2.5} - \frac{1}{5}\right\}\left.\frac{dX_1}{dt}\right\|_{nt-1}$	$\left.\frac{\partial X_1(noise)}{\partial t}\right\|_{nt} = 0.1$ $\left.\frac{\partial Y_1(noise)}{\partial t}\right\|_{nt} = -0.05$

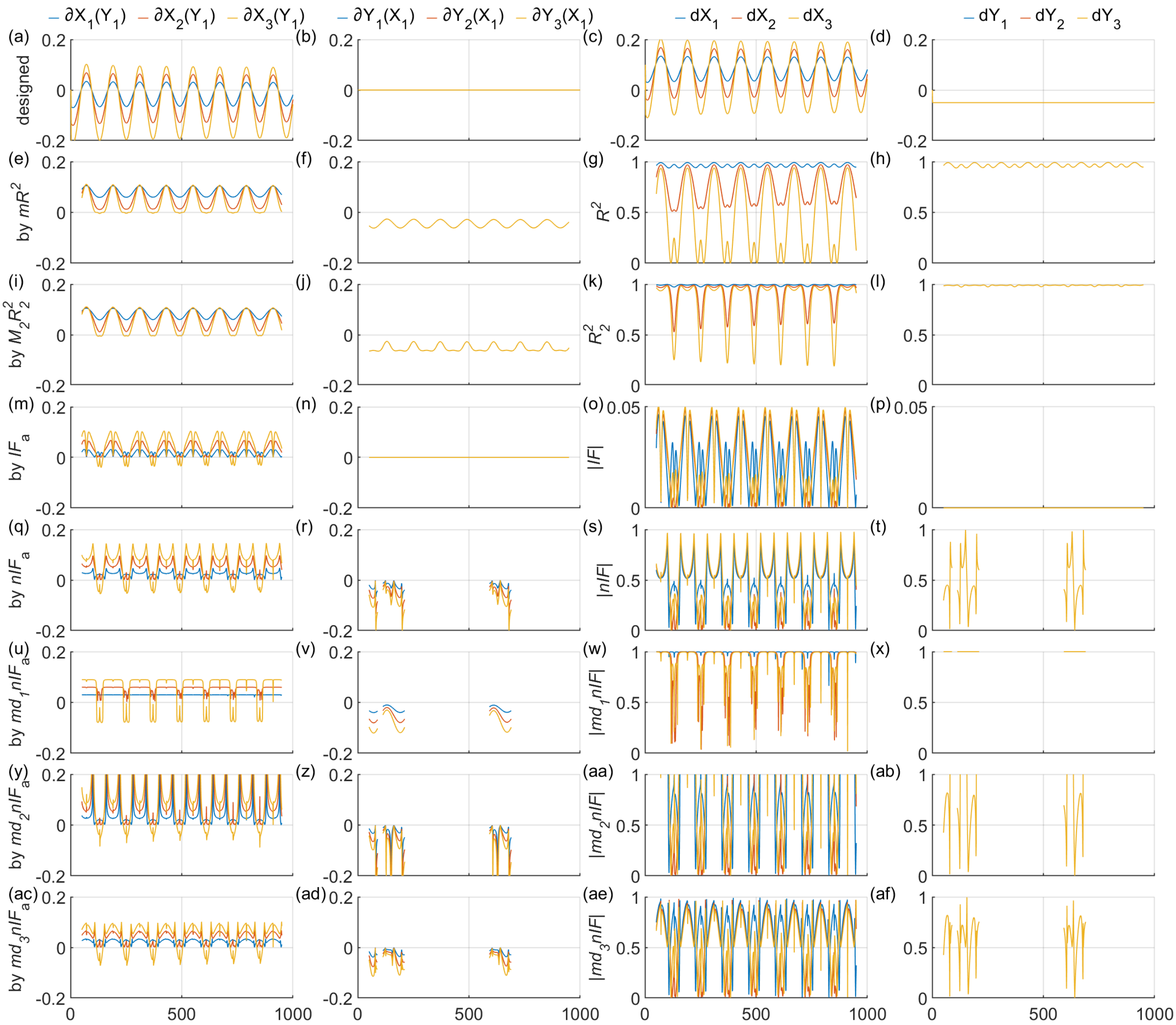

Figure S1. An 1D example with single-directional causality (Y→X) and a constant noise causing systematic bias (positive bias for *dX/dt* and negative bias for *dY/dt*). Two left columns: the designed (1st row) and estimated causal contributions. Two right columns: the designed change rate (1st row) and various R^2 or |multipliers| by different methods. It highlights the incapability of regressions to differentiate causal direction and to estimate negative contributions under positive bias. It also highlights the capability of IF_a to estimate the causal sensitivity. Other than IF_a, estimates by md_3nIF_a best fits to the designed trends. The sub-Figs a, b, ac, ad, are also the sub-Figs a-d in Fig. 2.

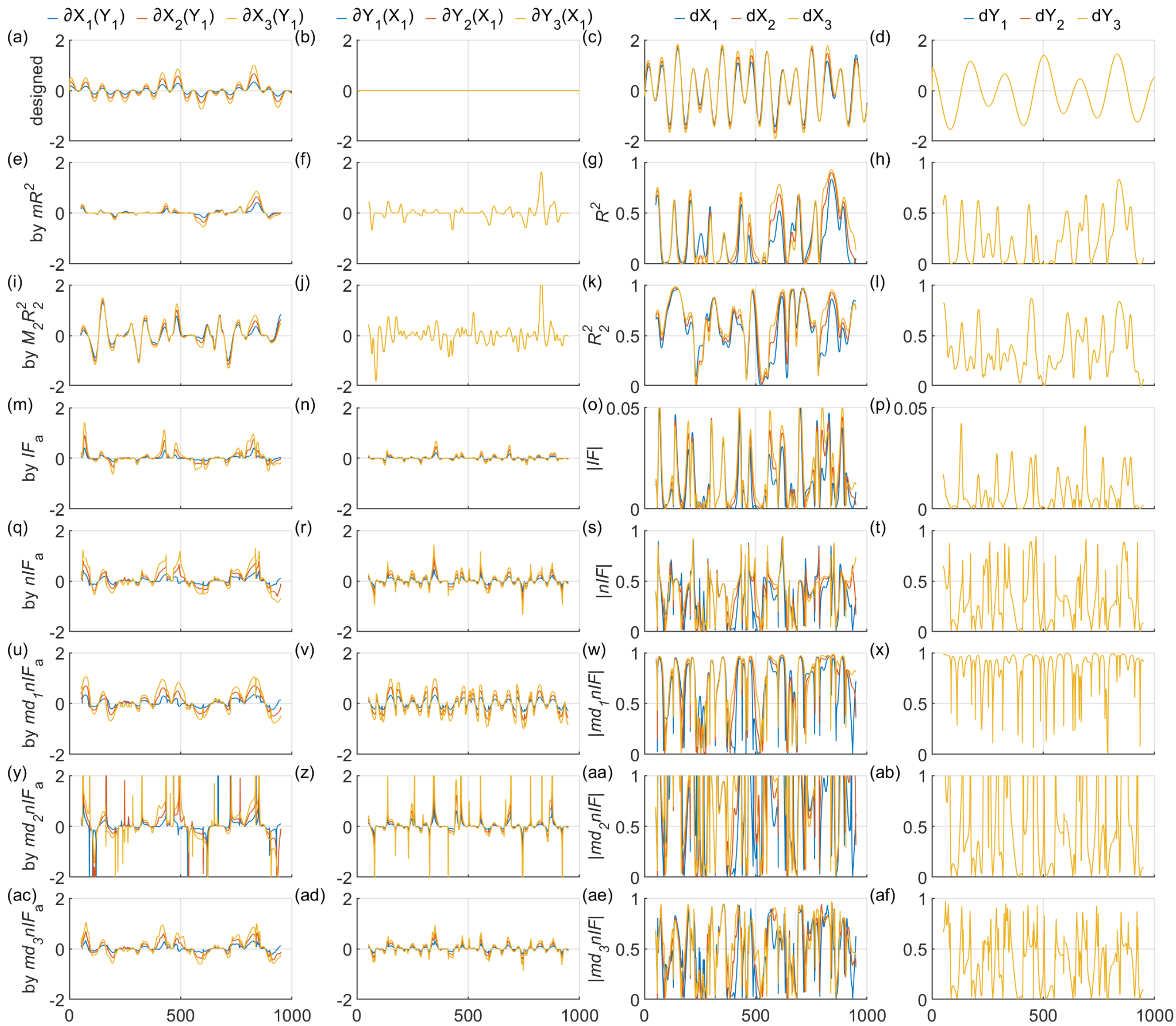

Figure S2. An 1D example with single-directional causality ($Y \rightarrow X$) and highly fluctuating independent noise contributions to dX/dt and dY/dt. Estimates by regressions are severely affected, losing both the peak-to-peak and the 1:2:3 ratios. For estimates by IF_a and various nIF_as, these ratios are still reasonably kept, with estimates by md_3nIF_a best representing the designed trends (from the perspectives of the two ratios and the width and shape of peaks). The sub-Figs a, b, ac, ad, are also the sub-Figs e-h in Fig. 2.

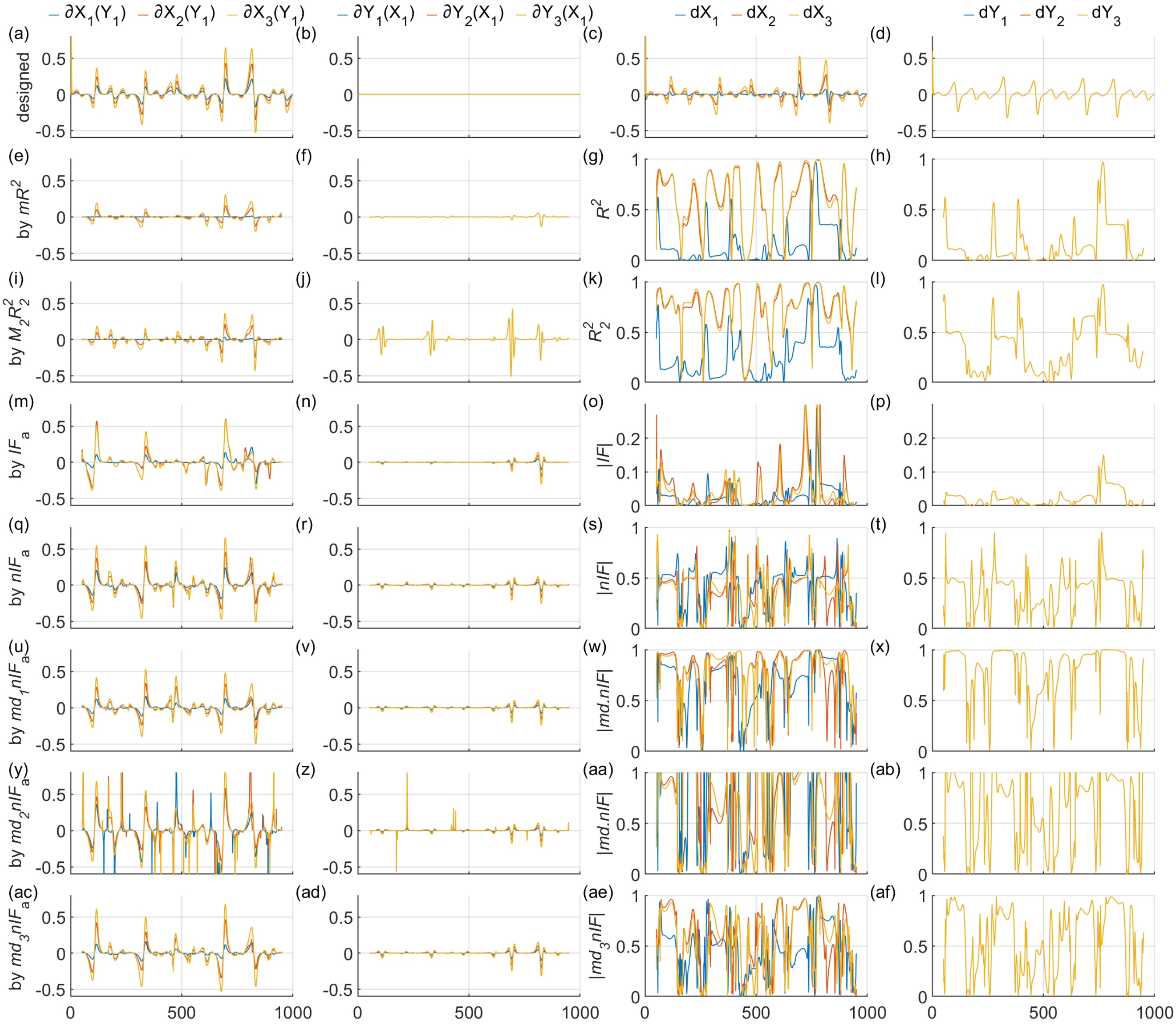

Figure S3. An 1D example with single-directional causality ($Y \rightarrow X$) and strongly oscillating self-dependency term contributions. The oscillating self-dependency terms change the 1:2:3 ratios for estimates by IF_a and md_2nIF_a. The peak-to-peak ratios for estimates by various nIF_a are also affected. Thus, it is difficult to differentiate which modification of *nIF* provides the better estimates. The sub-Figs a, b, ac, ad, are also the sub-Figs i-l in Fig. 2.

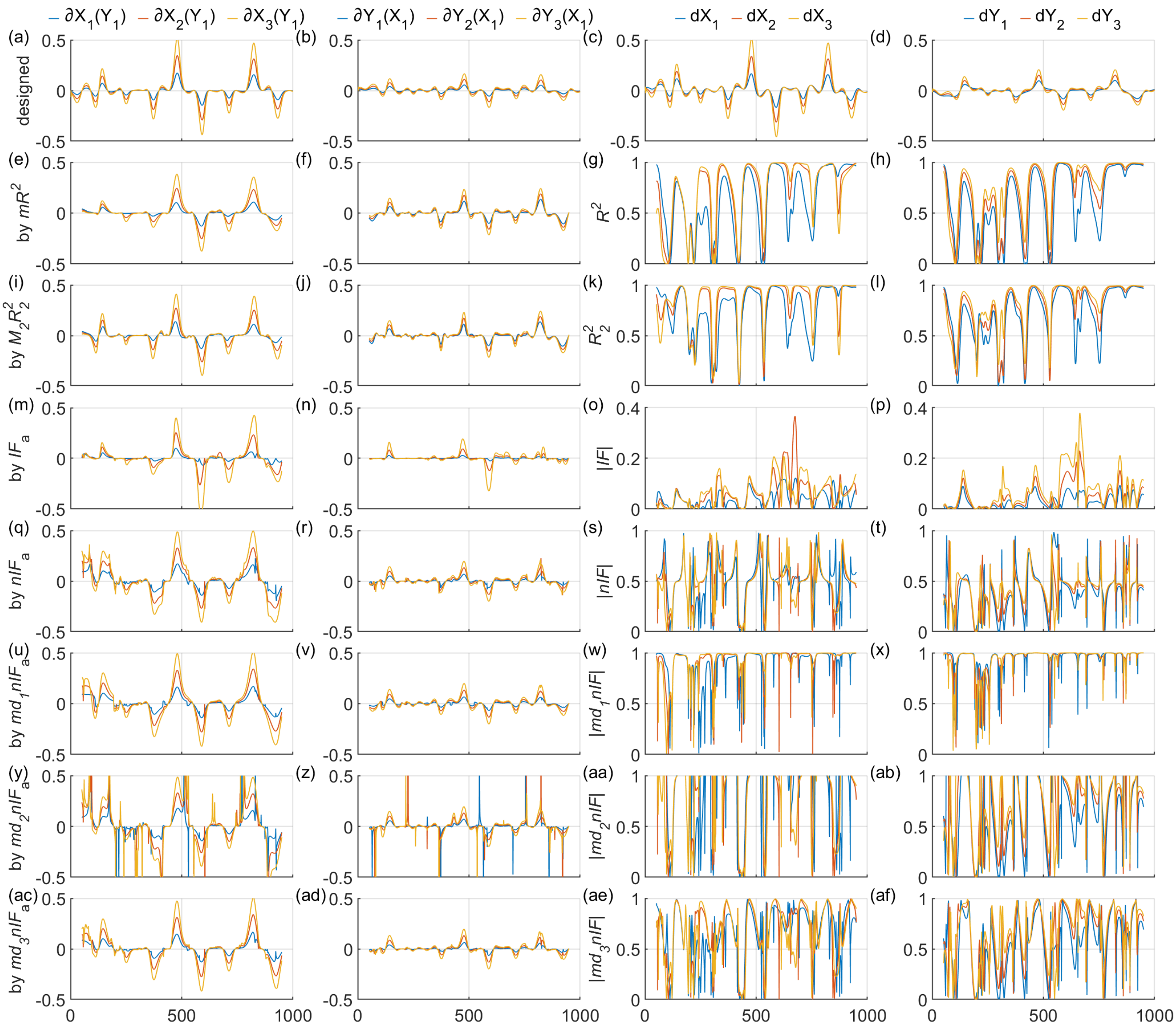

Figure S4. An 1D example with strong bidirectional causality but very weak self-dependency and independent contributions. The oscillating self-dependency terms change the 1:2:3 ratios for estimates by IF_a and md_2nIF_a. It highlights the lost 1:2:3 ratio for estimates by IF_a due to the bidirectional causality, and hence the peak-to-peak ratio too. The sub-Figs a, b, ac, ad, are also the sub-Figs m-p in Fig. 2.

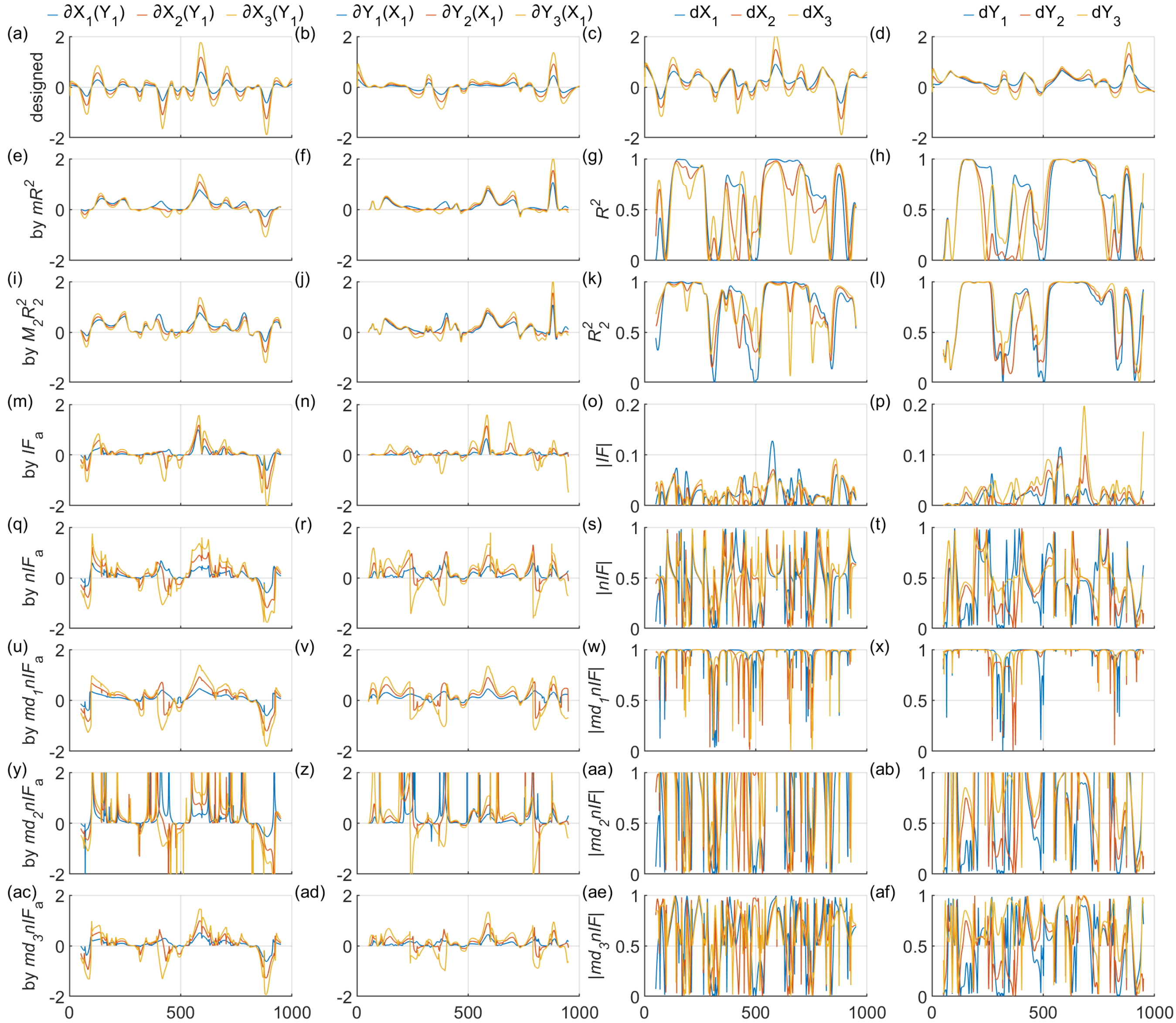

Figure S5. An 1D example with bidirectional causality and highly fluctuating independent noise contributions, creating fluctuating systematic bias and false correlation signs. The false correlation signs result in the designed -1:-2:-3 ratio of negative peaks to be misinterpreted ratio of ~3:2:1 by regressions and 1:2:3 by normalized information flows. Estimates by md_3nIF_a tends to minimize errors from the false correlation signs. The sub-Figs a, b, ac, ad, are also the sub-Figs q-t in Fig. 2.

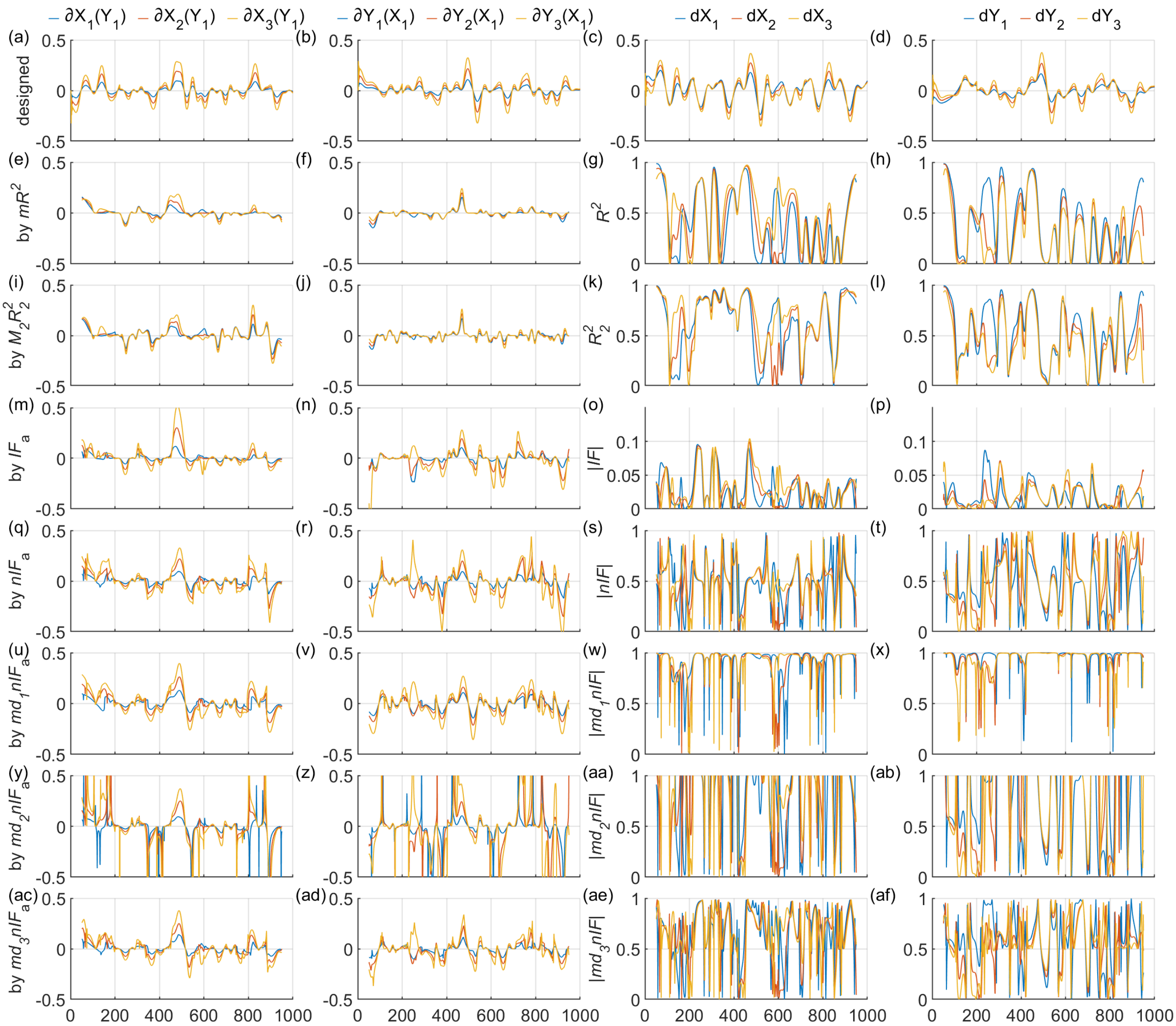

Figure S6. An 1D example with moderate bidirectional causality, self-dependency, and independent contributions, together with 21 units (21%) of time-lags for the interdependency terms from *t*>200. The estimates by md_1nIF_a and md_3nIF_a tend to provide the best fit and capture the ~21 unit of time-gaps from causes to effects. The sub-Figs a, b, ac, ad, are also the sub-Figs a-d in Fig. 3.

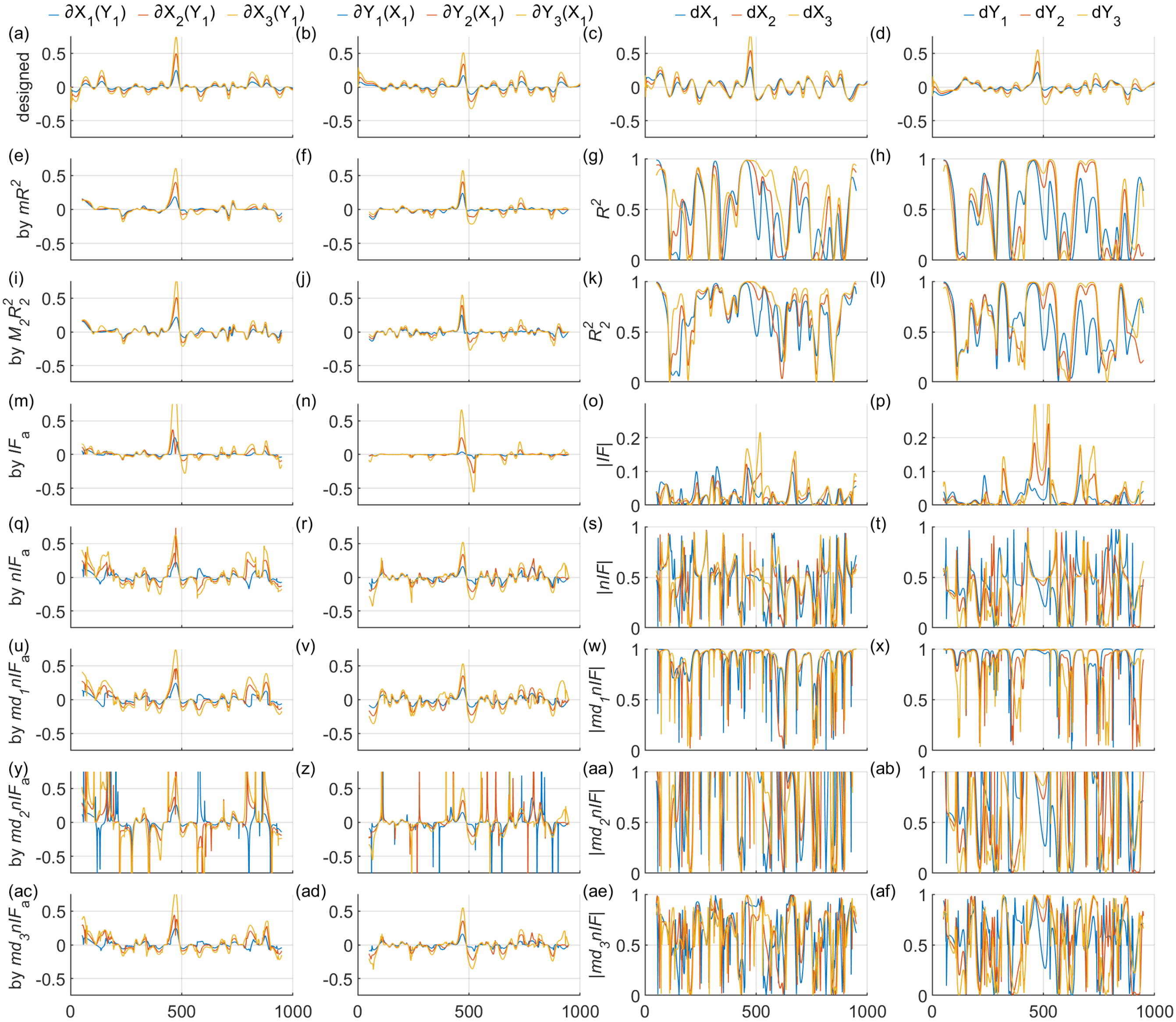

Figure S7. An 1D example with function modified from that for Fig. S6. It removes the time-lags for the interdependency terms. Estimates by regressions improve greatly due to the absence of time-lag and weak influence from noises. However, estimates by *IF* lose the 1:2:3 ratio as compared to Fig. S6, implying that the time-lag between interdependent causal contributions helps stabilize the denominator "overall |*IF*|" in equation 4.

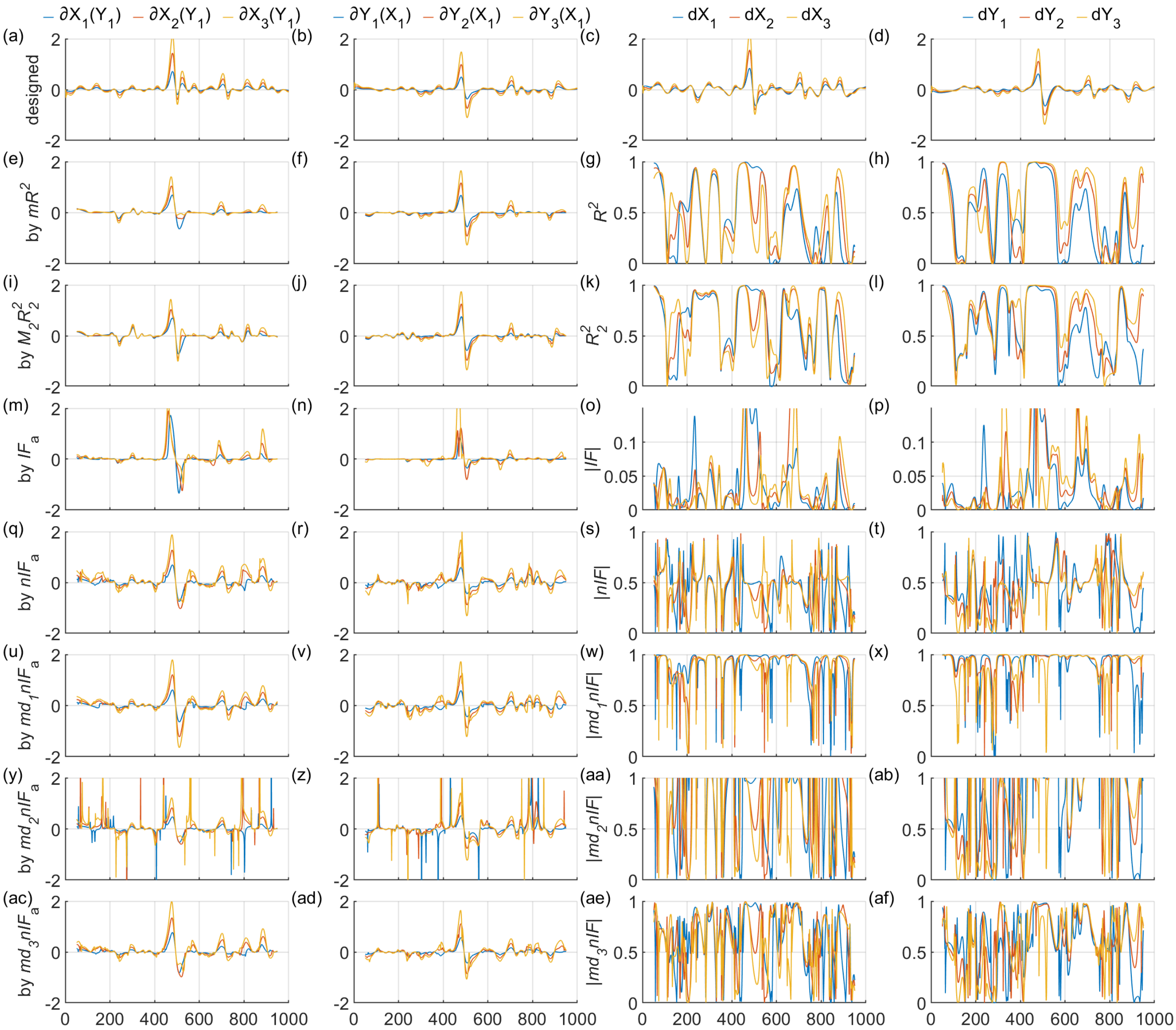

Figure S8. An 1D example with function modified from that for Fig. S6. It keeps the 21-unit time-lags only for the self-dependency terms. With the removal of time-lag for interdependency terms, estimates by regressions improve significantly. However, the time-lags for the self-dependency terms could significantly affect the estimates by (modified) nIF_a and IF_a, suggesting an increased difficulty in estimating the "overall $|IF|$" or the normalizing factor Z due to lagging contributions from self-dependency terms. The sub-Figs a, b, ac, ad, are also the sub-Figs e-h in Fig. 3.

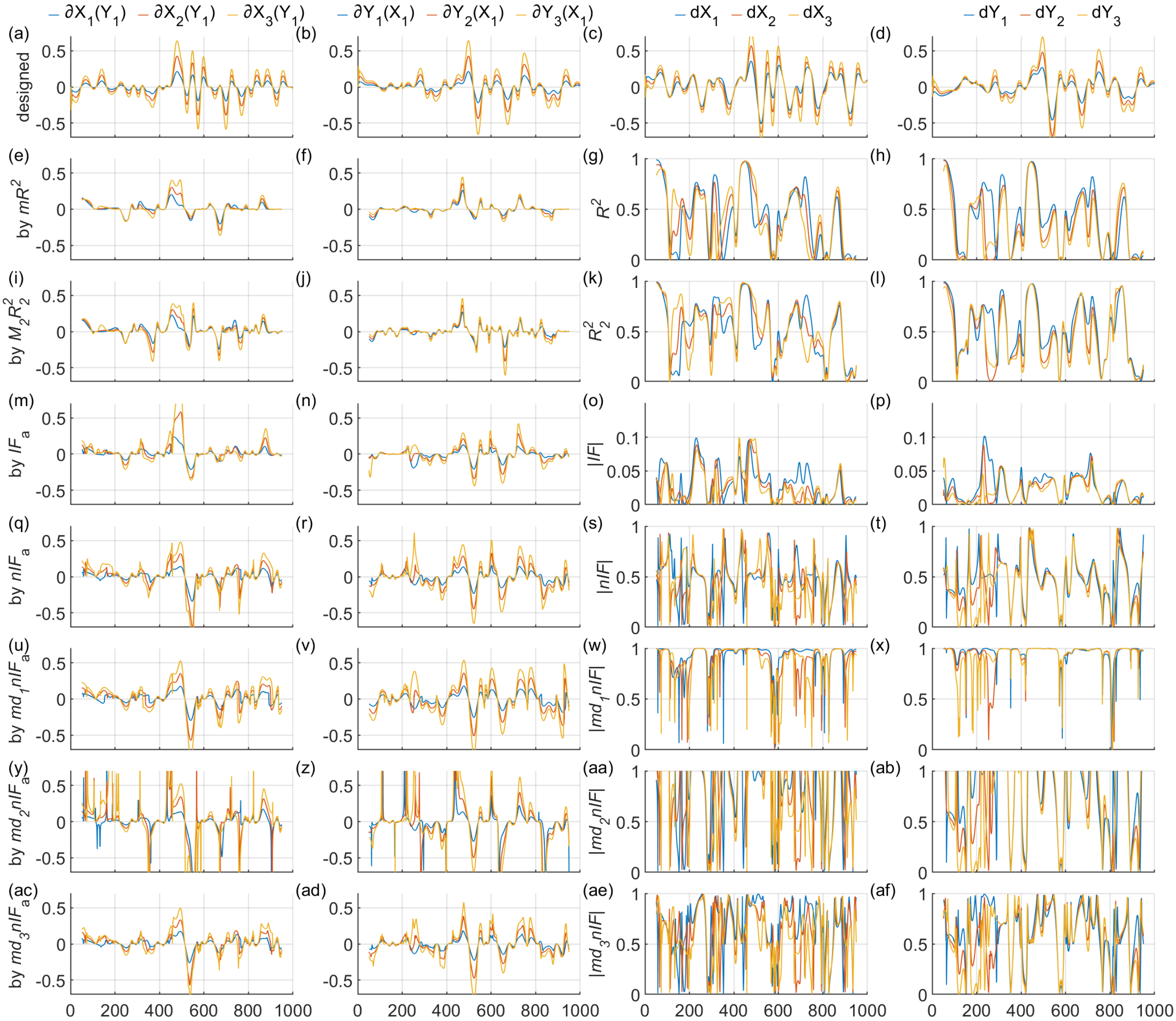

Figure S9. An 1D example with function modified from that for Fig. S6. It applies the 21-unit time-lags for both interdependency and self-dependency terms. Estimates by all the methods are significantly affected, including those given by (modified) nIF_a. However, while estimates by regressions and IF_a suffer poorer consistency for the 1:2:3 ratio and lose the peak-to-peak ratio, the estimates by (modified) nIF_a mainly suffer from the lost of accurate peak-to-peak ratios. The sub-Figs a, b, ac, ad, are also the sub-Figs i-l in Fig. 3.

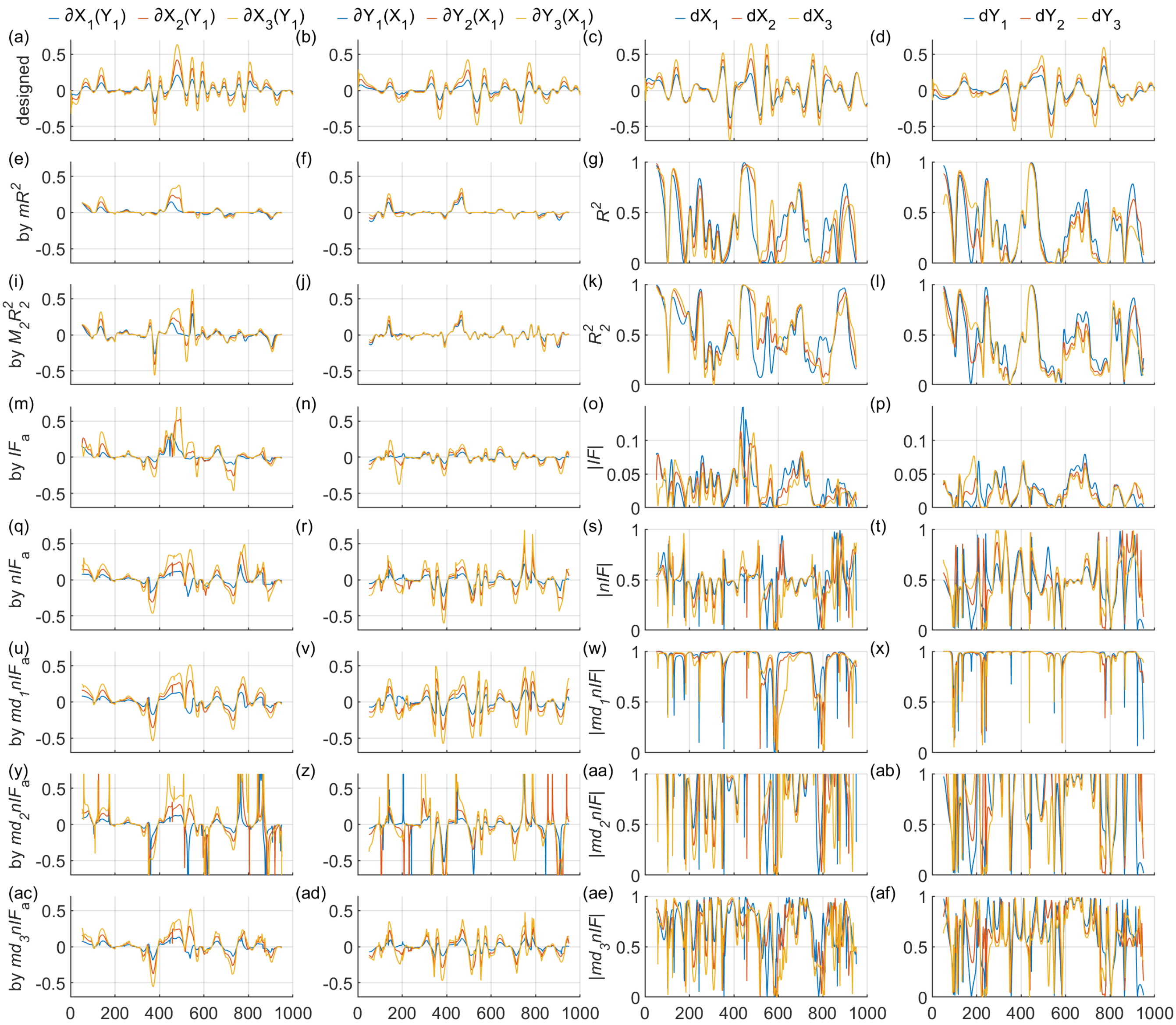

Figure S10. An 1D example with function modified from that for Fig. S6. The only difference is a slight change to one of the independent noise frequency terms, but it results merge (most in 1st column) and split (most in 2nd column) of the estimated causal contributions. The sub-Figs a, b, ac, ad, are also the sub-Figs m-p in Fig. 3.

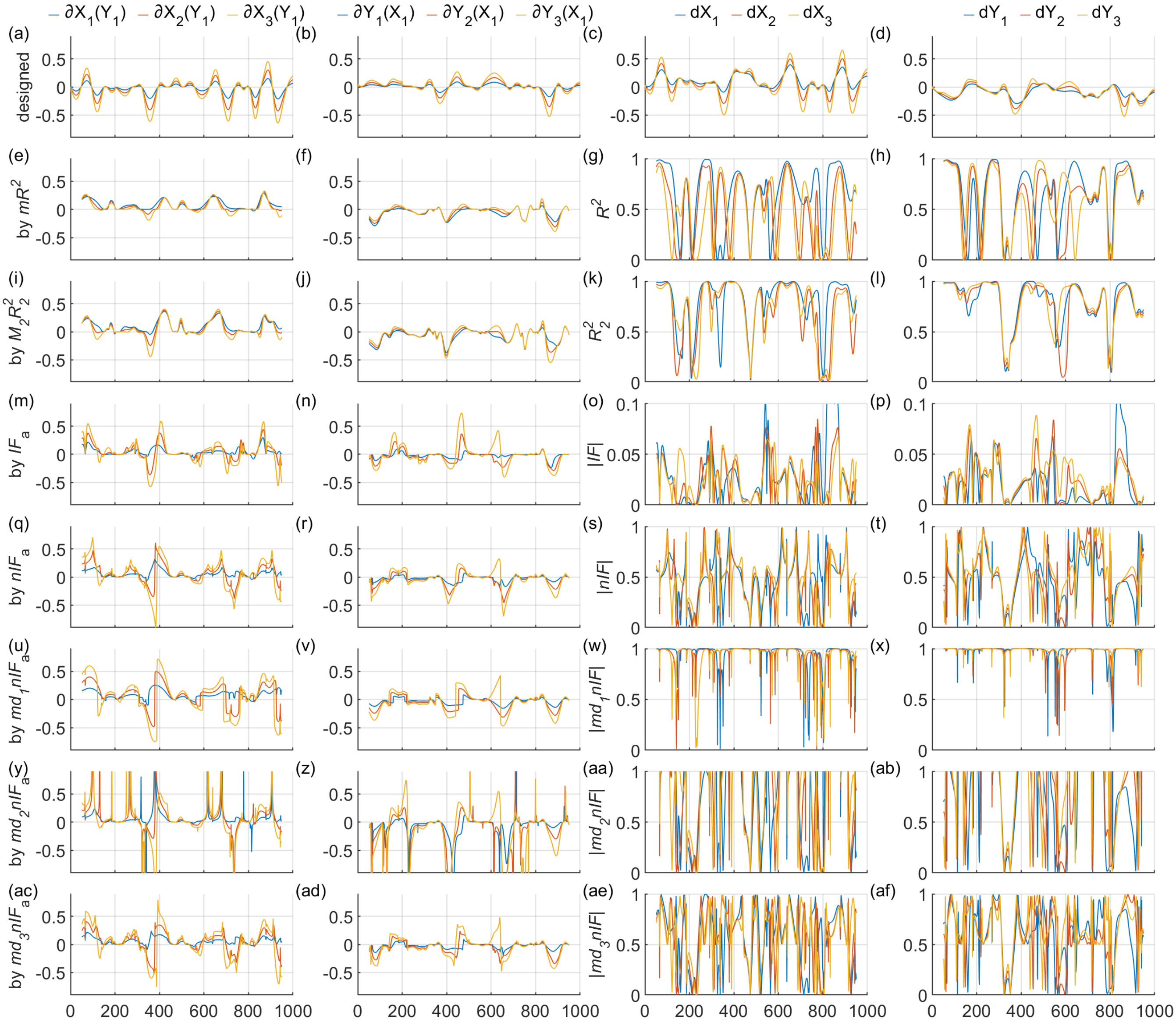

Figure S11. An 1D example with function modified from that for Fig. S6. It changes the 21-unit time-lags for the effects in the interdependency terms to become 31-unit time-lead. That is, effects leading causes by 31 time-units. The self-dependency terms are removed, and the independent noise term is slightly reduced to a lower magnitude and frequency. The estimated causal contributions, especially those by (modified) *nIF*$_a$ also tend to lag their designed peaks. This shows the estimated causal contributions do not only potentially reflect the effects lagging causes as in Fig. S6, but also extreme case with effects leading causes. This supports the hypothesis of normalized information flow to describe the normalized causal sensitivity at different times. The sub-Figs a, b, ac, ad, are also the sub-Figs q-t in Fig. 3.

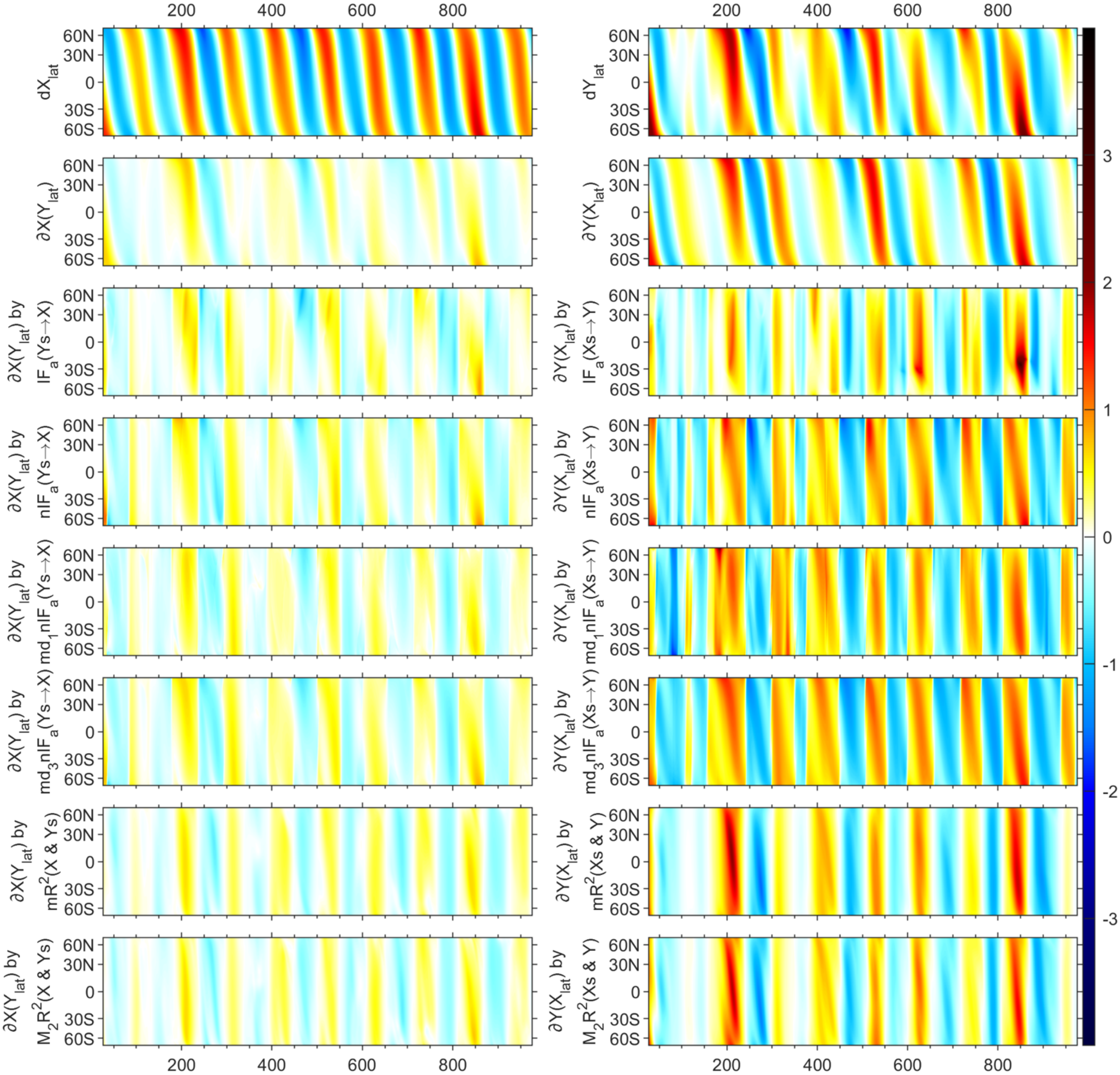

Figure S12. 3D-to-1D estimated cause-maps (3rd row and below) without the N-S teleconnections, which are supposed to duplicate the image of designed effect maps (2nd row). The 1st row shows the designed rates of changes, including contributions from noises. Like Fig. 4, the pattern across the latitudes is still best captured by the method using *md₃nIFₐ*. The mirroring teleconnection is best captured by *md₃nIFₐ*. However, for the peak-to-peak ratio across the time-axis, regressions are better when the noise level is low (right column).

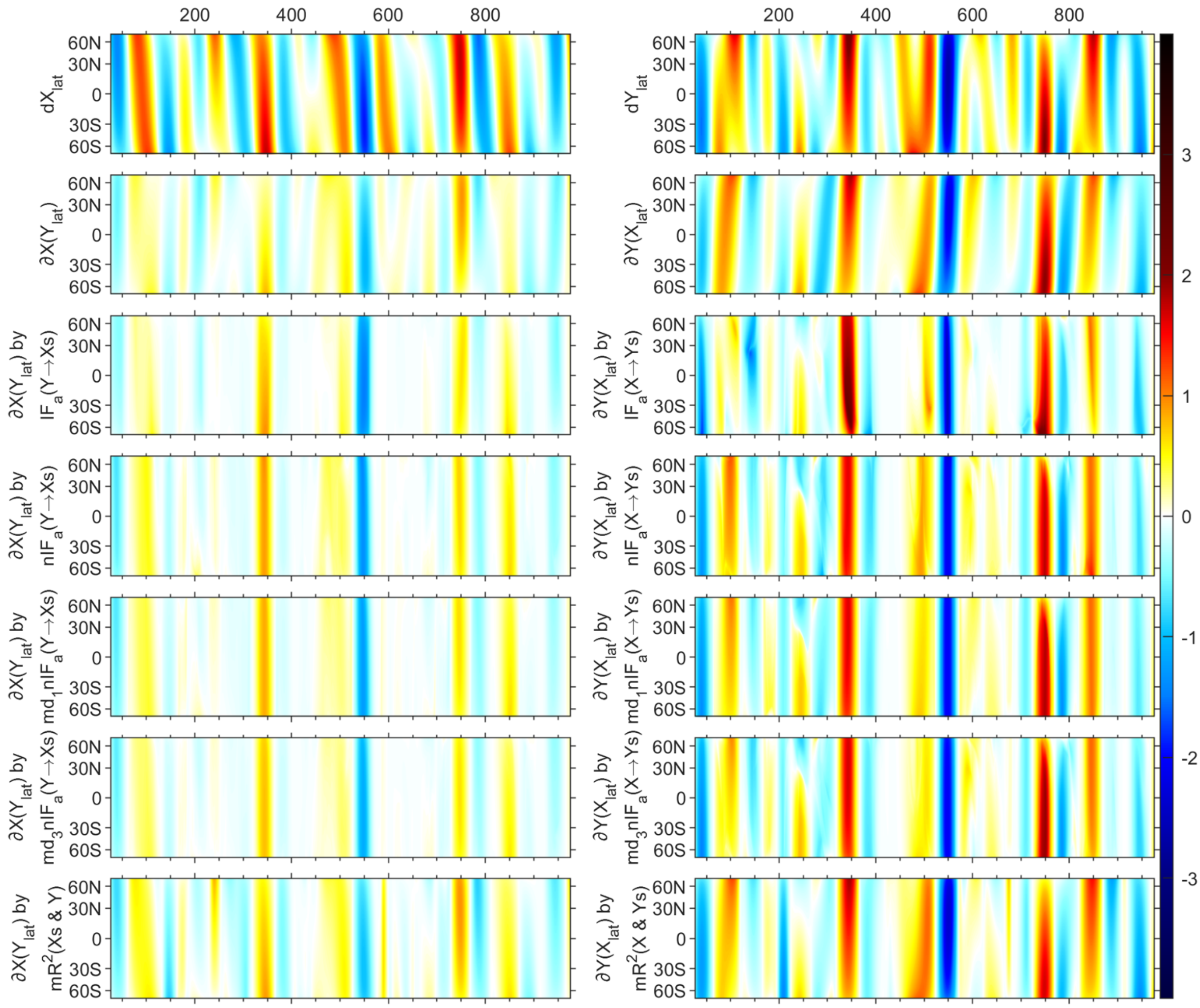

Figure S13. 1D-to-3D estimated effect-maps (3rd row and below) with the N-S teleconnections. Since the estimates are to show the 3D effects from just 1D time-series, the estimates are supposed to reflect the designed effect maps (2nd row). The benefit of using (modified) *nIF$_a$* in Fig. 4 is hence lost, while the issues about peak-to-peak ratio remains.

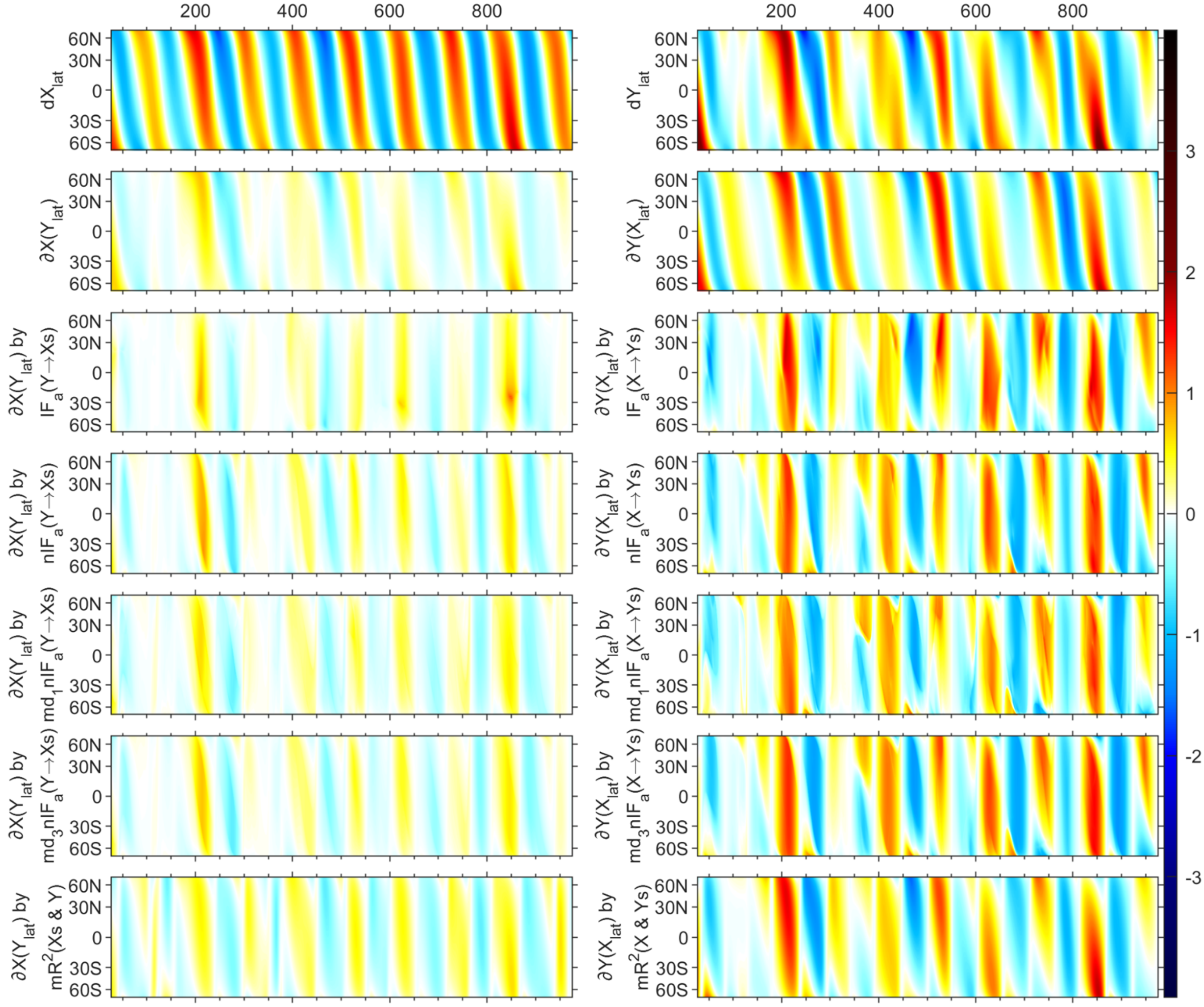

Figure S14. 1D-to-3D estimated effect-maps (3rd row and below) without the N-S teleconnections. Like Fig. S13, the benefit of identifying spatial distributions of causal contributions by using (modified) nIF_a is lost. However, with large independent noise-contributions (left column), estimates by (modified) nIF_a may still be more accurate than that by regressions.

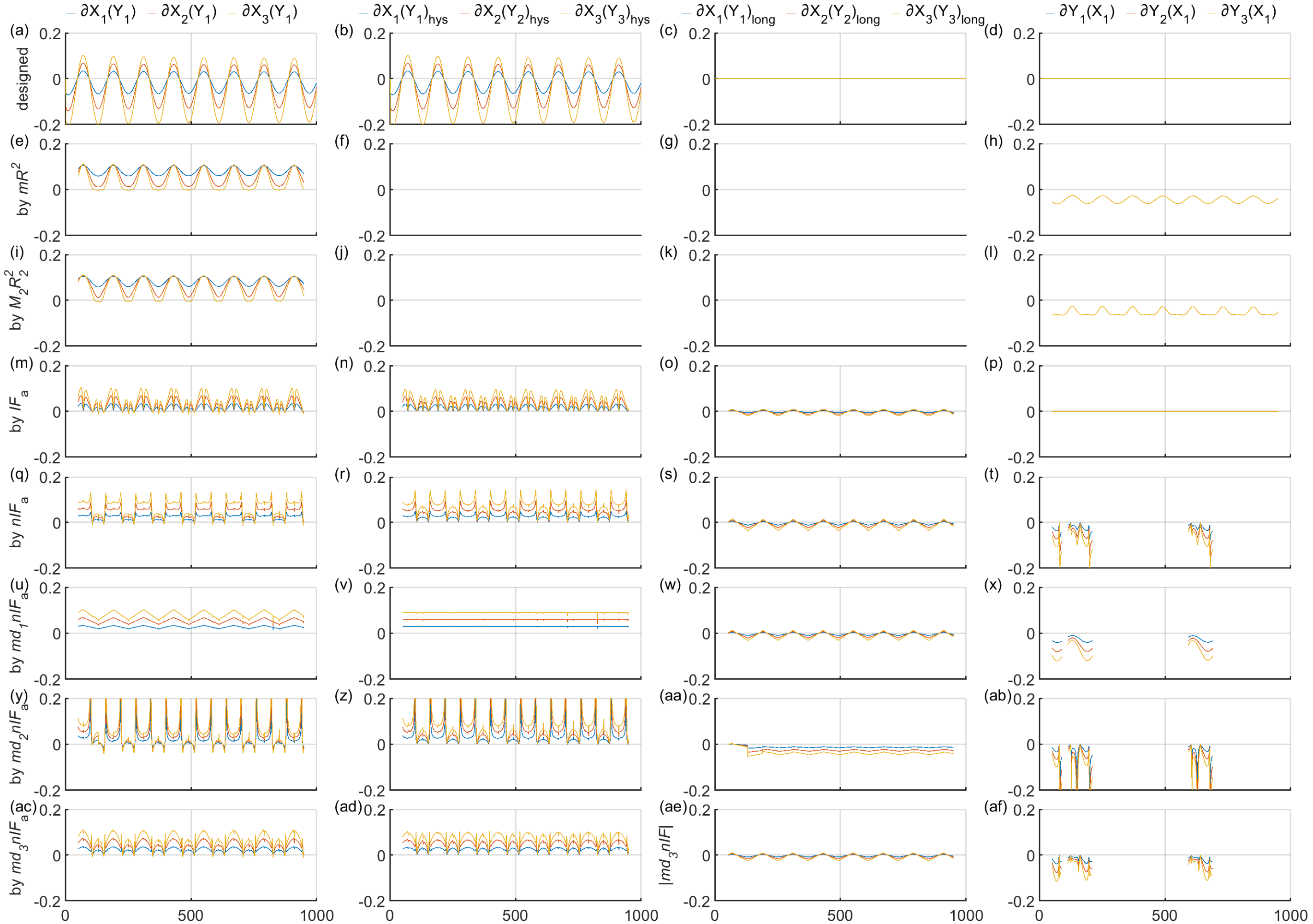

Figure S15. A single-directional 1D example with the same designed function as in Fig. S1, therefore the 2nd (and sub-Figs e,i) and 4th columns here are equivalent to the 1st and 2nd columns in Fig. S1, respectively). However, an assumed long-term $\partial X_{long}(Y)/\partial t$ (3rd column) is considered (which is zero in designed trend, sub-Fig. c) and added with the $\partial X_{hys}(Y)/\partial t$ (as the $\partial X(Y)/\partial t$ in Fig. S1) to form the $\partial X(Y)/\partial t$ (1st column). Note that sub-Figs f, g, j, k are left empty because for regressions we do not consider the $\partial X_{long}(Y)/\partial t$ based on X and Y time series.

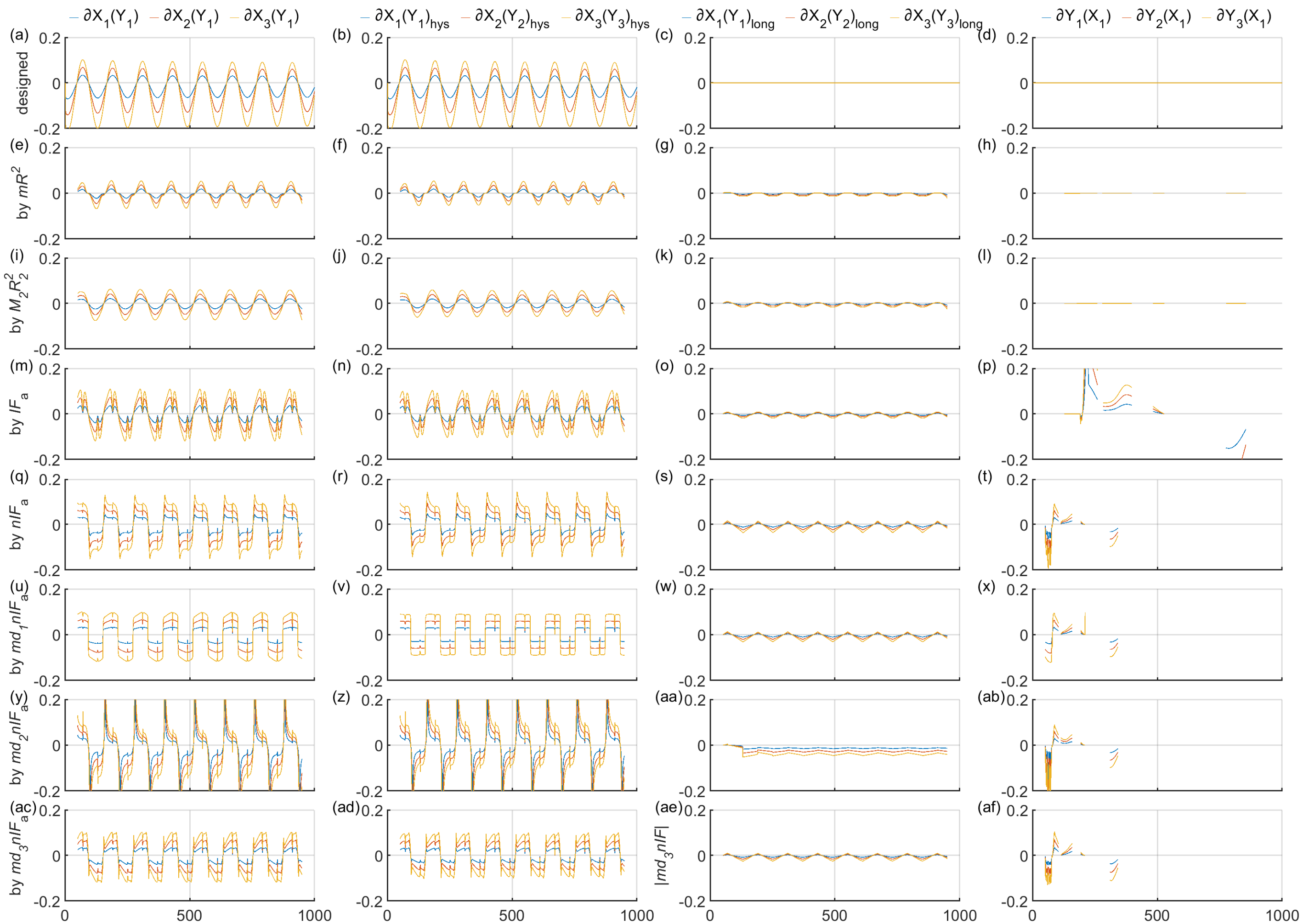

Figure S16. A single-directional 1D example with the same designed function and figure layout as in Fig. S15, but the estimates (2nd row and below) are based on X_{adj} and Y (first three columns) and X and Y_{adj} (last column). The dX_{ref}/dt is subtracted from dX/dt to obtain dX_{adj}/dt and eventually X_{adj}, and similarly dY_{ref}/dt is subtracted from dY/dt to obtain dY_{adj}/dt and eventually Y_{adj}. The calibration factor α is also kept as in Fig.S15. Compared to Fig. S15, a smaller magnitude of X_{adj} than X results in a milder oscillation for the estimated $\partial X_{hys}(Y)/\partial t$ based on regressions (i, n); but for estimated $\partial X_{hys}(Y)/\partial t$ based on *IF* and (modified) *nIF*s, the removal of dX_{ref}/dt helps minimize the errors due to independent noise, and correct most wrong correlation sign (n, r, v, z, ad). Note that for sub-Figs f, g, j, k, we still try to show $\partial X_{hys}(Y)/\partial t$ based on regressions of X_{adj} and Y, and $\partial X_{long}(Y)/\partial t$ based on regressions of dX/dt and Y.

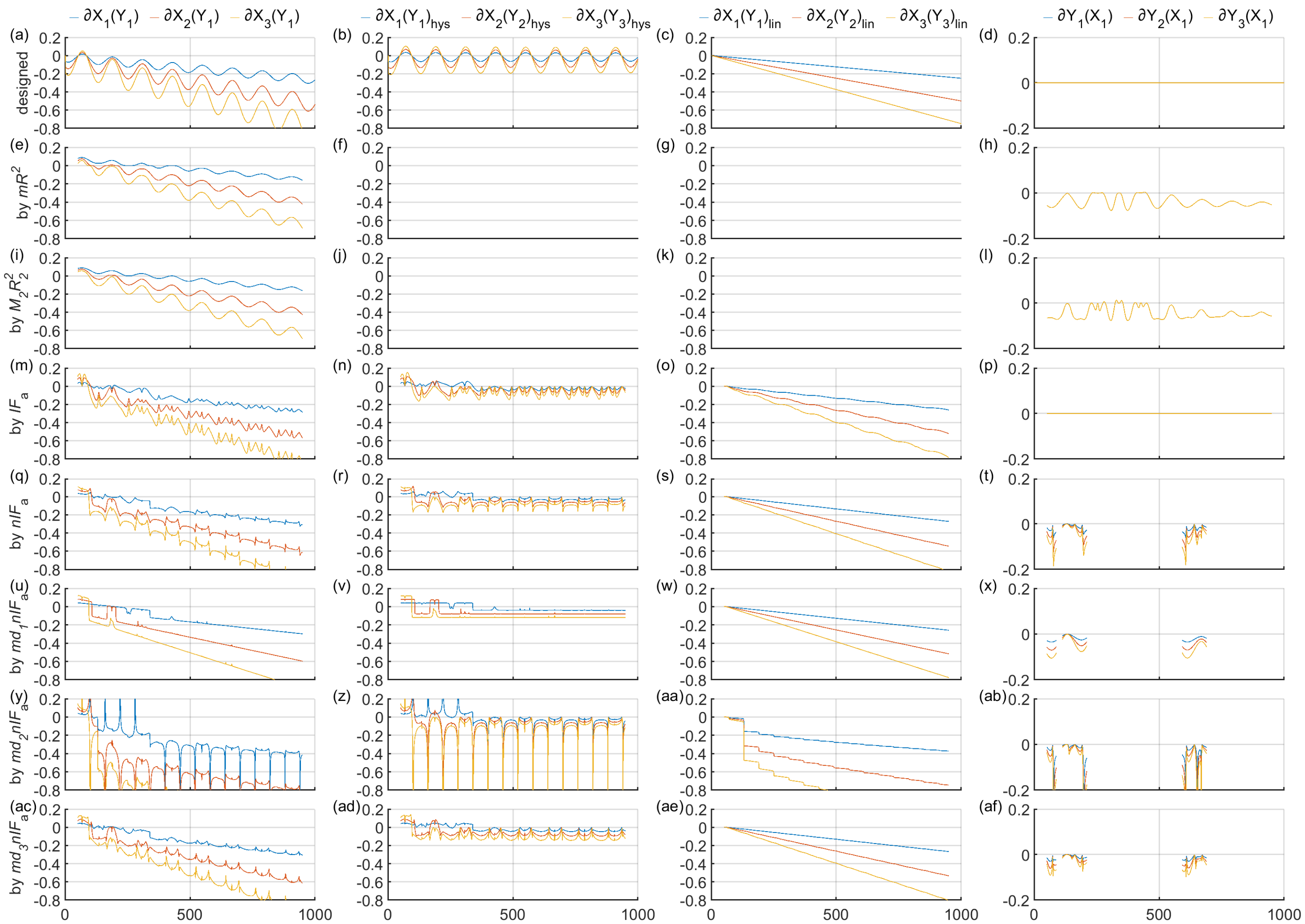

Figure S17. A single-directional 1D example with a growing negative $\partial X_{long}(Y)/\partial t$ added to the designed function in Fig. S15, with the estimates based on X and Y time series for $\partial X_{hys}(Y)/\partial t$ and $\partial Y(X)/\partial t$, and based on dX/dt and Y time series with subsequent integration for the $\partial X_{long}(Y)/\partial t$.

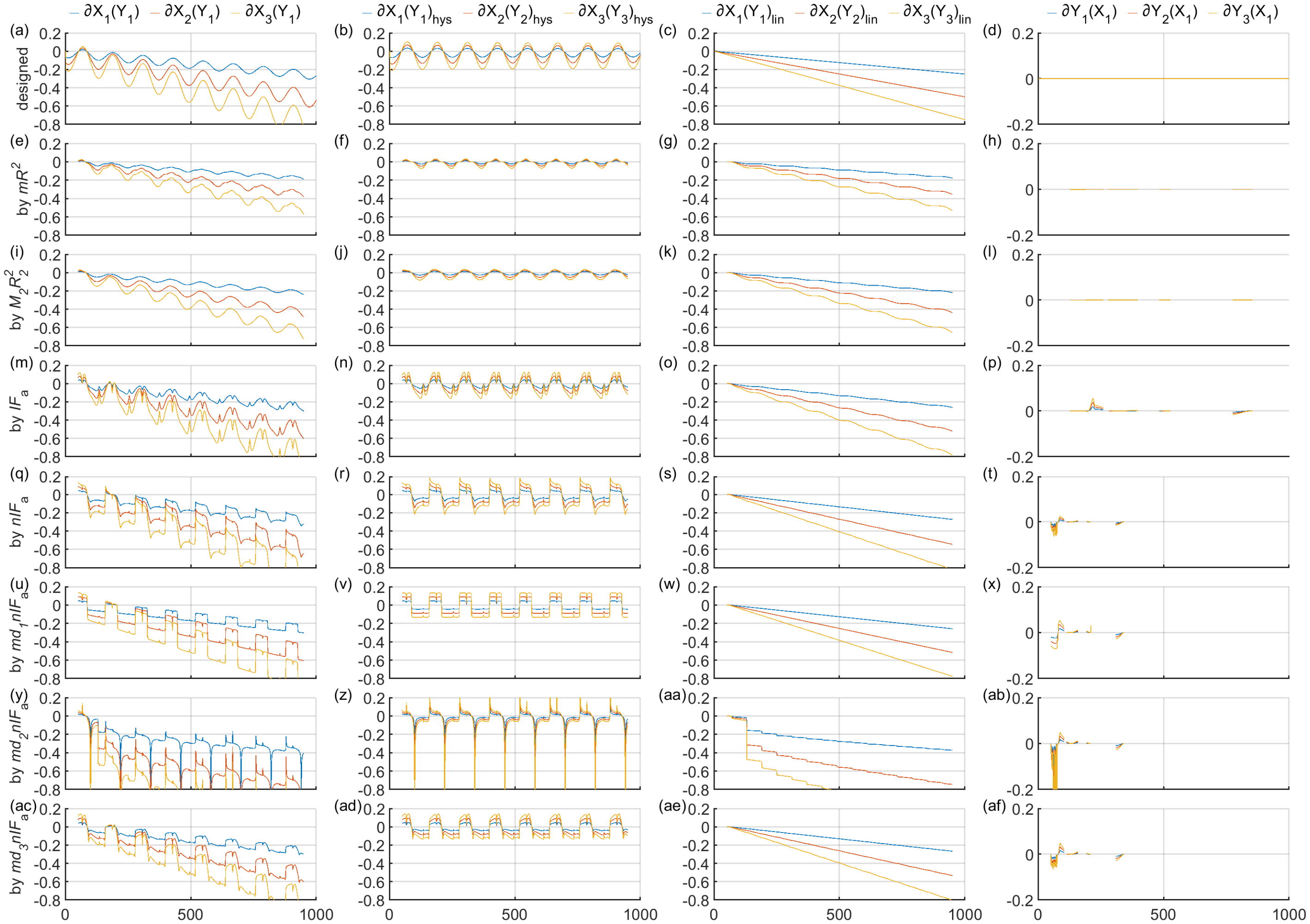

Figure S18. A single-directional 1D example with a growing negative $\partial X_{long}(Y)/\partial t$ as in Fig. S17, with $\partial X_{hys}(Y)/\partial t$ estimated based on X_{adj} and Y time series, $\partial Y(X)/\partial t$ estimated based on X and Y_{adj} time series, and $\partial X_{long}(Y)/\partial t$ estimated based on dX/dt and Y time series with subsequent integration for the $\partial X_{long}(Y)/\partial t$. The comparison between Fig.S17 and Fig.S18 is similar to that between Fig.S15 and Fig.S16: the use of X_{adj} instead of X helps improve the estimates of $\partial X_{hys}(Y)/\partial t$ given by *IF* and (modified) *nIF*s. On the other hands, although the $\partial X(Y)/\partial t$ given by regressions (e, i) may also reasonably reflect the designed trends, the oscillation of its estimated $\partial X_{hys}(Y)/\partial t$ component (f,j) is milder than the designed trends (b).

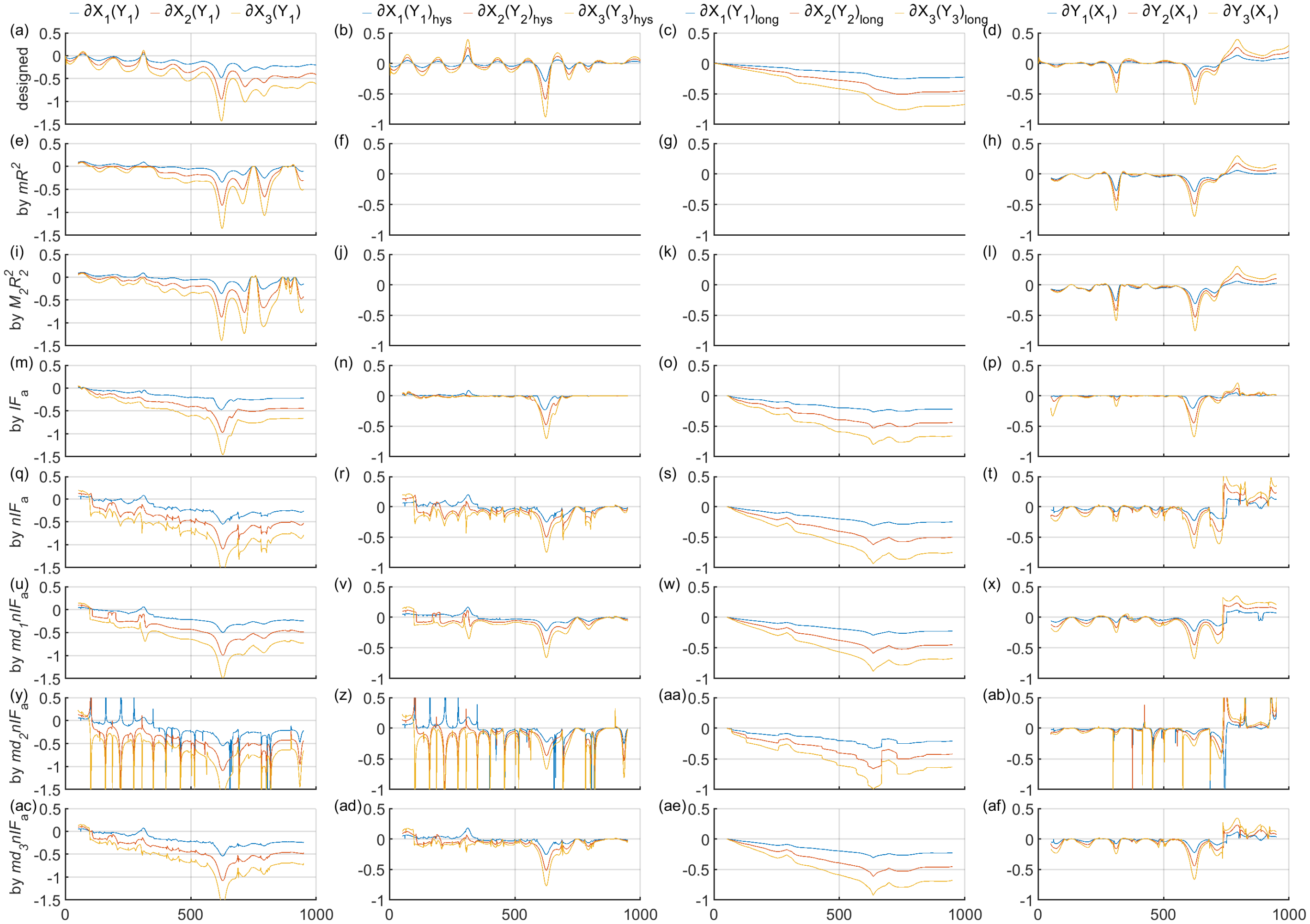

Figure S19. A single-directional 1D example with extended designed functions from Fig. S16-S17 by a coupled $\partial Y(X)/\partial t$ contribution, with the estimates based on X and Y time series for $\partial X_{hys}(Y)/\partial t$ and $\partial Y(X)/\partial t$, and based on dX/dt and Y time series with subsequent integration for the $\partial X_{long}(Y)/\partial t$.

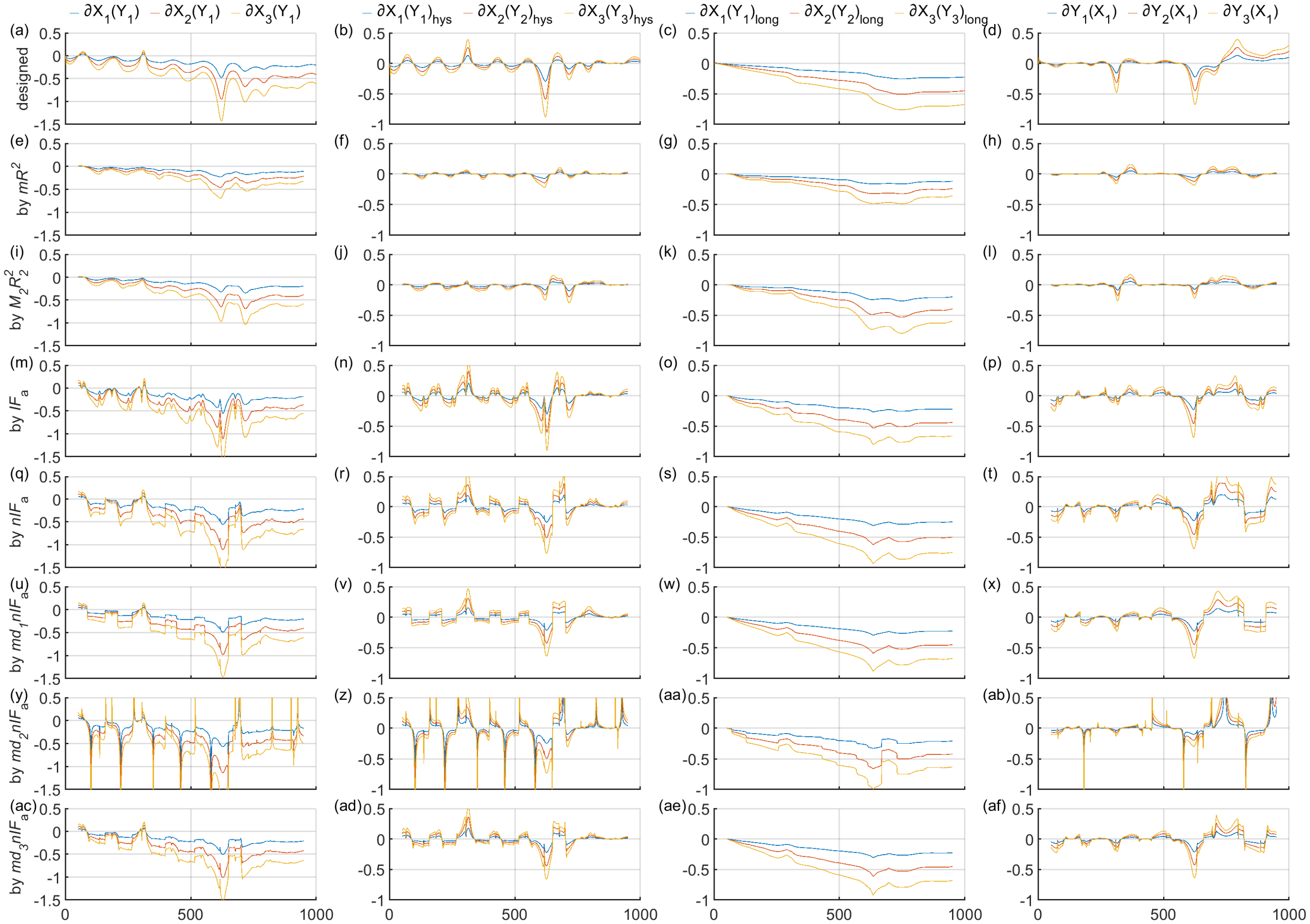

Figure S20. A single-directional 1D example with designed functions as in Fig.S19, with $\partial X_{hys}(Y)/\partial t$ estimated based on X_{adj} and Y time series, $\partial Y(X)/\partial t$ estimated based on X and Y_{adj} time series, and $\partial X_{long}(Y)/\partial t$ estimated based on dX/dt and Y time series with subsequent integration for the $\partial X_{long}(Y)/\partial t$. The comparison between Fig.S19 and Fig.S20 is similar to that between Fig.S17 and Fig.S18: the use of X_{adj} instead of X helps improve the estimates of $\partial X_{hys}(Y)/\partial t$ given by *IF* and (modified) *nIF*s but not that given by regressions. Nevertheless, the use of Y_{adj} instead of Y deteriorates the estimates of $\partial Y(X)/\partial t$.

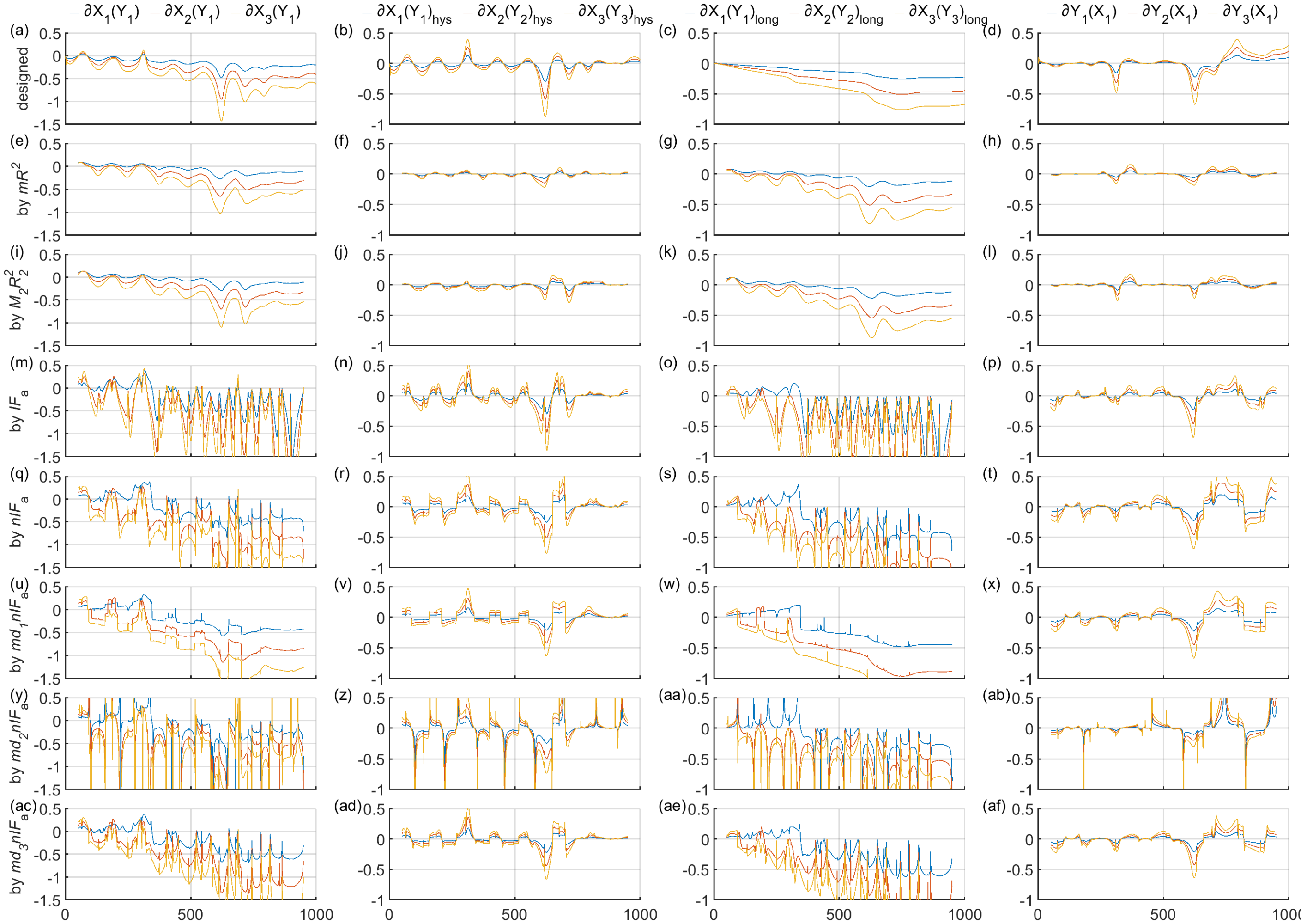

Figure S21. A single-directional 1D example with designed functions as in Fig.S19 and S20. However, the $\partial X_{long}(Y)/\partial t$ is estimated based on X and integral of Y followed by multiplication to the Y (instead of estimates of multipliers based on dX/dt and Y, followed by multiplication of dY/dt and subsequent integration, i.e. equation 20, adopted for Figs.S17-S20). This alternate approach appears to improve the $\partial X(Y)/\partial t$ by regressions (e, i) but such improvement is not via improving the estimates of individual subcomponents (f, g, j, k). On the other hands, the $\partial X_{long}(Y)/\partial t$ estimated by *IF* and (modified) *nIF*s appear highly fluctuating (o, s, w, aa, ae, note that the calibration factors were kept as in Fig. S20). The correlation sign may also be influenced by the sign of $\partial X_{hys}(Y)/\partial t$ (e.g. at time < 300 the blue line in each subfigure becomes positive, and similarly, the red and orange lines are positive at time <100).